

1 **Intra- and inter-annual changes in isoprene emission from central Amazonia**

2

3 Eliane Gomes Alves^{1,2*}, Raoni Aquino Santana³, Cléo Quaresma Dias-Junior^{4,2}, Santiago
4 Botía⁵, Tyeen Taylor⁶, Ana Maria Yáñez-Serrano^{7,8,9}, Jürgen Kesselmeier¹⁰, Pedro Ivo
5 Lembo Silveira de Assis¹¹, Giordane Martins¹¹, Rodrigo de Souza¹², Sergio Duvoisin
6 Junior¹³, Alex Guenther¹⁴, Dasa Gu¹⁵, Anywhere Tsokankunku¹⁶, Matthias Sörgel¹⁶, Bruce
7 Nelson¹⁷, Davieliton Pinto¹¹, Shujiro Komiya¹, Diogo Martins Rosa¹¹, Bettina Weber^{18,10},
8 Cybelli Barbosa^{10,18}, Michelle Robin¹, Kenneth J Feeley¹⁹, Alvaro Duque²⁰, Viviana
9 Londoño Lemos²¹, Maria Paula Contreras²², Alvaro Idarraga²³, Norberto López A.²³, Chad
10 Husby²⁴, Brett Jestrow²⁴.

11

12 ¹ Department of Biogeochemical Processes, Max Planck Institute for Biogeochemistry, Jena, Germany

13 ² Climate and Environment Department, National Institute of Amazonian Research, Manaus, Brazil

14 ³ Department of Atmospheric Sciences, Federal University of Western Para, Santarem, Brazil

15 ⁴ Federal Institute of Para, Belem, Brazil

16 ⁵ Department of Biogeochemical Signals, Max Planck Institute for Biogeochemistry, Jena, Germany

17 ⁶ Department of Civil & Environmental Engineering, University of Michigan, USA.

18 ⁷ IDAEA-CSIC, 08034, Barcelona, Spain

19 ⁸ CREAM, E08193 Bellaterra (Cerdanyola del Vallès), Catalonia, Spain

20 ⁹ Global Ecology Unit, CREAM-CSIC-UAB, E08193 Bellaterra (Cerdanyola del Vallès), Catalonia, Spain

21 ¹⁰ Multiphase Chemistry Department, Max Planck Institute for Chemistry, Mainz, Germany

22 ¹¹ Department of Tropical Forest Sciences, National Institute for Amazonian Research, Manaus, Brazil

23 ¹² Meteorology Department, State University of Amazonas, Manaus, Brazil

24 ¹³ Chemistry Department, State University of Amazonas, Manaus, Brazil

25 ¹⁴ Department of Earth System Science, University of California, Irvine, U.S.A.

26 ¹⁵ Division of Environment and Sustainability, Hong Kong University of Science and Technology, Clear
27 Water Bay, Hong Kong, China

28 ¹⁶ Atmospheric Chemistry Department, Max Planck Institute for Chemistry, Mainz, Germany

29 ¹⁷ Coordination of Environmental Dynamics, National Institute of Amazonian Research, Manaus, Brazil

30 ¹⁸ Institute for Biology, Division of Plant Sciences, University of Graz, Graz, Austria

31 ¹⁹ Department of Biological Sciences, University of Miami, Coral Gables, FL, USA.

32 ²⁰ Departamento de Ciencias Forestales, Universidad Nacional de Colombia–Sede 19Medellín, Medellín,
33 Colombia

34 ²¹ Department of Plant and Microbial Biology, University of Minnesota, USA

35 ²² Jardín Botánico de Cartagena “Guillermo Piñeres”, Turbaco, Bolívar, Colombia.

36 ²³ Fundación Jardín Botánico de Medellín, Antioquia, Colombia.

37 ²⁴ Fairchild Tropical Botanic Garden, Miami, FL, USA

38 *egomes@bgc-jena.mpg.de

39

40

41

42

43

44

45



46 **Abstract**

47 Isoprene emissions are a key component in biosphere-atmosphere interactions, and the
48 most significant global source is the Amazon rainforest. However, intra- and inter-annual
49 variations in biological and environmental factors that regulate isoprene emission from
50 Amazonia are not well understood and, thereby, poorly represented in models. Here, with
51 datasets covering several years of measurements at the Amazon Tall Tower Observatory
52 (ATTO), in central Amazonia, Brazil, we (1) quantified canopy profiles of isoprene mixing
53 ratios across seasons of normal and anomalous years and related them to the main drivers
54 of isoprene emission – solar radiation, temperature, and leaf phenology; (2) evaluated the
55 effect of leaf age on the magnitude of the isoprene emission factor (E_s) from different tree
56 species and scaled up to canopy with intra- and inter-annual leaf age distribution derived
57 by a phenocam; and (3) adapted the leaf age algorithm from MEGAN with observed
58 changes in E_s across leaf ages. Our results showed that the variability in isoprene mixing
59 ratios was higher between seasons (max. during the dry-to-wet transition seasons) than
60 between years, with values from the extreme 2015 El-niño year not significantly higher
61 than in normal years. In addition, model runs considering in-situ observations of canopy E_s
62 and the modification on the leaf age algorithm with leaf-level observations of E_s presented
63 considerable improvements in the simulated isoprene flux. This shows that MEGAN
64 estimates of isoprene emission can be improved when biological processes are
65 mechanistically incorporated into the model.

66

67 **1. Introduction**

68

69 Isoprene dominates the emission of biogenic volatile organic compounds (BVOCs) into
70 the atmosphere, and its major global source is tropical vegetation (Guenther et al., 2012;
71 Sindelarova et al., 2014). In the atmosphere, isoprene is a short-lived (minutes to hours)
72 reactive BVOC species, and its photooxidation affects the atmospheric oxidation capacity
73 contributing to the formation of ozone (O_3) and secondary organic aerosols (SOA)
74 (Atkinson, 1997; Pöschl et al., 2010). With its high plant foliage biomass and rich plant
75 diversity (ter Steege et al., 2013), the Amazon Forest represents a key source of isoprene
76 to the atmosphere (Yáñez-Serrano et al., 2020). However, model estimates of isoprene
77 emission and its intra- and inter-annual variability in the Amazon still carry high
78 uncertainty, because only a few observational experiments have been conducted with
79 mechanistic and process-based approaches, which hinders further modeling optimization
80 (Alves et al., 2018; Yáñez-Serrano et al., 2020). One of the most critical knowledge gaps
81 is how plants' isoprene emission differs under extremely hot and dry conditions, such as in
82 El-niño years, and how this might affect atmospheric processes. As some studies have
83 indicated that extreme years will become more frequent and intense with climate change
84 (Nobre et al., 2016; Boulton et al., 2022), it is essential to understand the processes
85 mediated by isoprene in such years to improve model estimates (Yáñez-Serrano et al.,
86 2020; Artaxo et al., 2022).

87

88 Some reasons for uncertainties in isoprene model estimates are already known. The correct
89 determination of the magnitude of the isoprene source - or the emission factor at leaf
90 standard conditions ($1000 \mu\text{mol m}^{-2} \text{s}^{-1}$ photosynthetically active radiation- PAR, 30°C),
91 as it is conceptualized in models (e.g., Guenther et al., 1995) - is crucial to improve isoprene



92 modeling estimates. The Amazon plant biodiversity represents a considerable challenge for
93 determining the isoprene emission factor. Although previous studies suggested that ~ 1%
94 of tree species are hyperdominant - with their tree individuals responsible for half of all
95 tree stems, carbon storage, and productivity (ter Steege et al., 2013; Fauset et al., 2015) -,
96 it is still unclear which plant species can emit substantial amounts of isoprene (Monson et
97 al., 2013), how these isoprene emitters are distributed throughout the Amazon basin, and
98 how the isoprene emission factor varies seasonally and interannually as result of changes
99 in eco-physiological processes (Gomes Alves et al., 2022). Another source of uncertainty
100 is related to quantifying the main sinks of isoprene. Once emitted by plant foliage, isoprene
101 can undergo surface deposition onto plant canopy (Karl et al., 2004) and soil (Pegoraro et
102 al., 2006), can be oxidized at rates depending on the atmospheric concentration of other
103 gases such as NO_x, O₃ and OH (Atkinson, 1997), and can be transported into and out of the
104 atmospheric boundary layer (Wei et al., 2018). Additionally, the rapid conversion of
105 isoprene photooxidation products can open a further sink for BVOCs in plants. This
106 chemical and biological processing of emitted compounds may affect vertical transport
107 processes, again influencing the biosphere (Kesselmeier et al., 2002; Canaval et al., 2020).

108
109 In addition, seasonal variation in isoprene emission from Amazon forests has been reported
110 by several in-situ studies, with the indication that isoprene seasonality is driven by intra-
111 annual variation in solar radiation, temperature, and leaf phenology (Kuhn et al., 2004a, b;
112 Yáñez-Serrano et al., 2015; Alves et al., 2016, 2018; Wei et al., 2018; Langford et al.,
113 2022). On a larger scale, satellite retrievals of isoprene oxidation products, like
114 formaldehyde (Barkley et al., 2009; Bauwens et al., 2016), and direct retrieval of isoprene
115 (Fu et al., 2019; Wells et al., 2022) have given an initial view of the long-term Amazon
116 isoprene emission, enabling not only seasonal but also inter-annual comparisons. Yet, there
117 remains a need to parameterize and evaluate the estimations with local and regional
118 measurements and to gain a better understanding of the main processes related to sources
119 and sinks of isoprene, since some studies have shown that satellite-derived isoprene
120 emission values are either overestimated (Alves et al., 2016) or underestimated (Gu et al.,
121 2017), or even show maximum emissions in a different season when compared to in-situ
122 measurements (Alves et al., 2016, 2018).

123
124 Here we report in-situ observations of isoprene mixing ratios during different seasons and
125 in consecutive years in central Amazonia to evaluate intra- and inter-annual variabilities in
126 two normal years (2013-2014) and one El-niño year (2015); in addition, we report
127 observations of leaf-level isoprene emission factor and leaf phenology monitoring. With
128 the intra- and inter-annual observations of isoprene at a central Amazonian site, this study
129 proposes to: (1) quantify the isoprene mixing ratios across seasons of normal and
130 anomalous years and compare them with the main drivers of isoprene emission – solar
131 radiation, temperature, and leaf phenology; (2) evaluate the effect of leaf age on the
132 magnitude of the isoprene emission factor from different tree species and scale up with
133 canopy intra- and inter-annual leaf age distribution; and (3) use the Model of Emissions of
134 Gases and Aerosols from Nature (MEGAN) to assess the effects of the observed changes
135 in the isoprene emission factor across leaf ages, by modifying the leaf age algorithm and
136 comparing simulations with observations at canopy-level.

137



138 **2. Methods**

139 *2.1 Amazon Tall Tower Observatory (ATTO)*

140

141 We performed measurements at the ATTO site located 150 km northeast of Manaus in the
142 Uatumã Sustainable Development Reserve (USDR) in central Amazonia. The climate is
143 tropical humid, with two distinctive seasons – wet season (December-May) and dry season
144 (July-October) and transition seasons in between – and has a mean annual precipitation of
145 2380 mm (Botía et al., 2022). The vegetation in this area is considered mature, mostly
146 non-flooded rainforest (terra-firme), with a mean canopy height of 35 m, and
147 predominantly occurs on plateaus at a maximum altitude of approximately 130 m a.s.l.
148 (Andreae et al., 2015). Utmost air masses arriving at the site come from the east (NE~20%,
149 ENE~27%, E~33%, ESE~19%) (Zannoni et al., 2020) and have passed through 1500 km
150 of undisturbed terra-firme rainforest, with minor intrusion of air masses from Manaus
151 (Pöhlker et al., 2019). Figure 1 shows seasonal variation in solar radiation, air temperature,
152 precipitation, and soil moisture from 2013 to 2019. Andreae et al. (2015) have more details
153 on this experimental site.

154

155 *2.2 Mixing ratios of isoprene – canopy level*

156

157 Isoprene gradient mixing ratios were inferred by air samples collected from the INSTANT
158 tower (80 m height, coordinates: S 02°08.7520' W 58°59.9920') at eight heights in and
159 above the canopy (0.05, 0.5, 4, 12, 24, 38, 53 and 79 m) during intensive campaigns across
160 different seasons from November 2012 to October 2015. Eight heated (50 °C) and insulated
161 inlets (fluorinated ethylene propylene - FEP) were connected to a Proton Transfer Reaction
162 – Mass Spectrometer (PTRMS) (Ionicon Analytic GmbH, Austria), which was housed in
163 an air-conditioned container 10 m from the INSTANT tower. The inlets were guided to a
164 valve system, switching every 2 min between the different heights, completing a full profile
165 in 16 min. The mean total uncertainty of isoprene mixing ratios was 9.9 %, within the
166 PTRMS measurement uncertainty (~10%). For more details on the experimental setup,
167 PTRMS conditions, and calibration, we refer the reader to Yáñez-Serrano et al. (2015).

168

169 *2.3 Flux of isoprene – canopy level*

170

171 During a campaign in November 2015, eddy covariance fluxes of isoprene were measured
172 for 11 days. Isoprene concentrations were obtained with the above-described PTRMS at a
173 time resolution of 1 s and from a separate 3/8" inlet at 41 m height that sampled air at a
174 flow rate of about 10 l min⁻¹. A CSAT3 sonic anemometer (Campbell Scientific Inc.,
175 Logan, U.S.A.) measured the three-dimensional wind speed at high frequency and was
176 placed at a distance of 0.5 m from the isoprene inlet. Fluxes were then calculated by
177 correlating fluctuations of the vertical wind vector to the fluctuations of isoprene
178 concentrations with the software package EddyPro® (LI-COR Inc., Lincoln, U.S.A.). A
179 method for despiking and raw data statistical screening was employed (Vickers and Mahrt,
180 1997). Half-hourly averaged fluxes were flagged according to a method of data quality
181 control (Mauder and Foken, 2004), and only data with the highest quality (flags 0 and 1)
182 was used for further analyses. Losses for sampling frequencies between 0.1 and 0.8Hz have



183 been observed as below 10% (Guenther and Hills, 1998; Spirig et al., 2005; Holst et al.,
184 2010; Jensen et al., 2018). Footprints were calculated using a two-dimensional model for
185 a geographic domain of 2 x 2 km centered at the INSTANT tower (Kljun et al., 2015). The
186 Tovi Footprint Analysis Toolbox (LI-COR Inc., Lincoln, U.S.A.) was used to calculate
187 half-hourly footprints and to combine them for the measurement period. More details on
188 the flux measurements and data processing are given in Pfannerstill et al. (2018).

189

190 *2.4 Leaf Area Density – measurements with the Light Detection and Ranging sensor* 191 *(LiDAR)*

192

193 Measurements of canopy leaf area density were carried out with a ground Light Detection
194 and Ranging sensor (LiDAR) at the ATTO site. These measurements aimed to give
195 information on the canopy structure around the INSTANT tower. Ground-LiDAR surveys
196 were conducted in October 2015 with a Riegl LD90-3100VHS-FLP system (Horn,
197 Austria), which generated a canopy profile map in vertical and horizontal directions. We
198 walked ten transects of 150 m in length with the ground-LiDAR system, and measurements
199 were averaged every 15 m of each transect, summing up to ten measurements per transect.
200 Measurements of all ten transects were then averaged and presented with the confidence
201 interval (95%). More details about how the ground LiDAR data were analyzed can be
202 obtained from Stark et al. (2012).

203

204 *2.5 Leaf-level monitoring of leaf demography and phenology*

205

206 Leaf demography and phenology of 36 trees were monitored from March 2016 to
207 December 2017. Along 100 m of canopy walkways, canopy leaves were monitored
208 monthly to determine leaf ages and investigate how leaf age proportions vary during the
209 year. Ten branches of each tree were randomly selected and labeled with one iron ring at
210 their bottom end. All leaves attached from the bottom to the apical end were counted and
211 dated according to the day of observation. For the first observation, all leaves were assigned
212 with unknown age. In the following months, every time a new leaf was observed, the date
213 of observation was recorded for that specific leaf. For leaf age determination, the date of
214 the first observation of a new leaf was set back to 15 days before observation. The age was
215 calculated by the difference, in the number of days, between the first day and the last day
216 of observation, resulting in a number of days with a deviation of plus-minus 15 days. For
217 instance, if a new leaf was observed on 1st July 2017, the flushing date of this leaf was
218 assigned for 17th June 2017 (+/- 15 days). Then, all subsequent measurements considered
219 17th June 2017 as a date for leaf flushing, and aging was counted based on the number of
220 days that this leaf stayed attached to the branch.

221

222 *2.6 Isoprene emission factor – leaf level*

223

224 Leaves of 21 canopy tree species, out of the 36 trees monitored for leaf demography and
225 phenology (described in section 2.5), were measured to determine the isoprene emission
226 factor across different leaf ages (Table S1) from October to November 2017. The other 15
227 trees were unreachable with the sampling system and, therefore, not measured. Leaf-level
228 isoprene sampling was carried out in 2-3 leaves of each age class available for each tree



229 during the measurement period, using a commercial portable gas exchange system GFS-
230 3000 (Walz, Effelthich, Germany). Each leaf was separately enclosed in the leaf chamber
231 at standard conditions – photosynthetic photon flux density (PPFD) set to 1000 $\mu\text{mol m}^{-2}$
232 s^{-1} and leaf temperature to 30°C - until net assimilation, stomatal conductance and internal
233 CO_2 concentration were stable. The measurement stability criterion was assigned as one
234 standard deviation of the net assimilation mean. The airflow rate going into the leaf
235 chamber was 400 $\mu\text{mol s}^{-1}$ and CO_2 and H_2O concentrations were 400 $\mu\text{mol.mol}^{-1}$ and 21
236 mmol.mol^{-1} (relative humidity of ~60%), respectively. Air exiting the GFS-3000 leaf
237 chamber was routed to fill sorbent cartridges (stainless steel tubes filled with Tenax TA
238 and Carbograph 5 TD sorbents), and a downstream pump sampled the exiting air at a rate
239 of 200 sccm for 10 min. A hydrocarbon filter (Restek Pure Chromatography, Restek
240 Corporations, USA) was installed at the air inlet of GFS-3000 to remove isoprene from the
241 incoming ambient air, and all tubing in contact with the sampling air was made of PTFE.
242 Before each measurement, a blank sample was obtained from the empty leaf chamber.

243
244 Isoprene content in the sorbent cartridges was determined by laboratory analysis at the
245 University of California (Irvine, U.S.A.). All cartridges were placed into a thermally
246 desorbing autosampler (TD-100, Markes International, Inc). The isoprene was pre-
247 concentrated at 10 °C followed by injection into a gas chromatograph (GC, model 7890B,
248 Agilent Technologies, Inc) equipped with a time-of-flight mass spectrometer (Markes
249 BenchTOF-SeV) and a flame ionization detector (TD-GC-FID/TOF-MS) (Woolfenden
250 and McClenny, 1999; ASTM D6196-15, 2015). Internal standards tetramethylethylene
251 and decahydronaphthalene were injected into each sample after collection and before
252 analysis. The system was calibrated daily with a commercial isoprene standard from Apel
253 Riemer Environmental Inc. The external gas standard was prepared using a dynamic
254 dilution system, and the effluent was added to sorbent cartridges under conditions similar
255 to those used for sampling. Once the volume mixing ratio of isoprene (ppbv) was obtained,
256 leaf emission flux was determined using the Eq. (1):

257
258
$$F = R_{ppbv} \times \frac{Q}{A} \quad (1)$$

259
260 where F ($\text{nmol.m}^{-2}.\text{s}^{-1}$) is leaf flux of isoprene emission; R_{ppbv} (nmol.mol^{-1}) is isoprene
261 concentration of the sample (cartridge); Q is the flow rate of air into the leaf chamber (400
262 $\mu\text{mol.s}^{-1}$); and A is the area of leaf within the chamber (0.08 m^2). The isoprene emission
263 rate was then calculated and converted to $\text{mg.m}^{-2}.\text{h}^{-1}$. For more details on tree species, leaf
264 age, and assigned leaf age class, see Table S1 in Supplementary Information.

265
266 *2.7 Tower-camera derived leaf phenology and demography data*

267
268 Upper canopy leaf phenology was monitored with a Stardot RGB camera (model Netcam
269 XL 3MP) installed at 81m height on the ATTO INSTANT tower. For more details on the
270 camera setup, radiometric calibration, and detection of phenological stages, we refer the
271 reader to Lopes et al. (2016). Only images acquired near noon and under an overcast sky
272 (diffuse illumination) were selected for subsequent analysis. The camera (subsequently
273 called phenocam) monitored the upper crown surfaces of 194 trees from July 2013 to



274 November 2018. Images were analyzed to track the temporal trajectory of each tree crown
275 and assign them into one of three classes: “leaf flushing” (crowns that showed a strong
276 increase in greening), “leaf abscising” (crowns which showed a large increase in greying,
277 which is the color of bare upper canopy branches) or “no change”. By counting the number
278 of individual trees per month for each category (flushing or abscission), we aggregated our
279 census to the monthly scale. Of the monitored trees, 69% ($n = 134$) had clear flushing and
280 abscission patterns, and, using the number of days after each flushing event, we determined
281 leaf age classes and attributed a fraction of the upper canopy crowns to an age class at
282 monthly intervals. We defined the following leaf age classes: (i) young leaves (0–1
283 month), (ii) growing (1–2 months), (iii) mature leaves (3–6 months), and (iv) old leaves
284 (>6 months). Then, we partitioned the age classes into classes of leaf area index (LAI)
285 (i.e., young, growing, mature, and old LAI) by normalizing each leaf age class with the
286 total LAI measured at ATTO. A constant LAI of $5.32 \text{ m}^2 \text{ m}^{-2}$ was used for all months,
287 since the variability of this number throughout the year was not statistically significant
288 (unpublished results). For the normalization, we considered the total number of trees in
289 the camera frame ($n = 194$), assuming that the 31% that do not have clear flushing patterns
290 are part of the old age class. For more details on the methods and assumptions for
291 separating LAI into leaf age classes, see Wu et al. (2016). Datasets of flushing and
292 abscission (<http://doi.org/10.17871/atto.223.7.840>) and the raw LAI age classes (<http://doi.org/10.17871/atto.230.4.842>).
293

294

295 *2.8 Isoprene emission trait – tree species level*

296

297 To get more detailed information on the trees monitored with the camera, a total of 194
298 trees were taxonomically identified, and the isoprene emission trait was assigned. Isoprene
299 emission data were obtained from published data and new measurements for the study
300 species. New measurements were conducted at the ATTO research site (described in
301 section 2.6), and additional measurements were obtained using the PORCO method (Taylor
302 et al., 2021), a customized photoionization detection system, on trees in tropical botanical
303 gardens. Briefly, all PORCO measurements were made in situ on uncut ‘sun’ branches by
304 enclosing one-to-few leaves inside rigid leaf cuvettes, acclimating them to darkness, and
305 then exposing the leaves to photosynthetically active radiation controlled at $1000 \mu\text{mol m}^{-2}$
306 s^{-1} , and temperatures near 30°C , for 3.5 minutes of measurement time. Emission rates
307 were corrected to a 30°C equivalent based on a standard temperature response curve
308 (Guenther et al., 1993). Emission rates exceeding $1 \text{ nmol m}^{-2} \text{ s}^{-1}$ were considered positively
309 indicative of isoprene emissions. See the full method validation and a discussion of the
310 rarity of detection of other compounds as false positives for isoprene in Taylor et al. (2021).
311 Botanic gardens used for tree measurements were: A. Duque private collection, Retiro,
312 Antioquia, Colombia; Fairchild Tropical Botanical Garden, Miami, FL, USA; Jardín
313 Botánico de Cartagena “Guillermo Piñeres”, Turbaco, Bolívar, Colombia; Jardín Botánico
314 “Joaquín Antonio Uribe” de Medellín, Antioquia, Colombia; Montgomery Botanical
315 Garden, Miami, FL, USA; Universidad Nacional de Medellín–Sede Medellín arboretum,
316 Antioquia, Colombia.

317

318 For applying isoprene measurements from external datasets (botanic garden measurements
319 or published literature) to our study species, we followed the methods of Taylor et al.,



320 (2018, 2019). We used data compiled from 12 literature sources (Bracho-Nunez et al.,
321 2013; Geron et al., 2002; Harley et al., 2004; Keller & Lerdau, 1999; Klinger et al., 1998;
322 Klinger et al., 2002; Lerdau & Keller 1997; Padhy & Varshney, 2005; Tambunan et al.,
323 2006; Taylor et al., 2018; Taylor et al., 2021; Varshney & Singh, 2003). Tree species
324 taxonomy was standardized by the Taxonomic Name Resolution Service (Boyle et al.,
325 2013; Boyle et al., 2021). We assigned species data only in terms of the genetically
326 determined capacity to produce isoprene (Monson et al., 2013); we did not consider the
327 variability in the strength of emissions, for which data are more limited and potentially
328 confounded by method variation and species plasticity. A species-level emission status–
329 emitter or non-emitter–was applied where available in external datasets; otherwise, genus-
330 level information was used to impute the emission status to unmeasured species. The
331 proportion of measured species in a genus that emit isoprene was used as an estimate of
332 the probability (p_{IE}) that any species sampled from the genus would be an emitter. For a
333 genus corresponding to one of our study species, for $p_{IE} \leq 1/3$, the species was estimated
334 to be a non-emitter, and for $p_{IE} \geq 2/3$, the species was estimated to be an emitter. For values
335 $1/3 < p_{IE} < 2/3$, the genus average was considered ambiguous and the species was excluded
336 from the analyses. Whereas there is some expected error in the assignment of emission
337 status to any given species, analyses of large numbers of species will tend toward the
338 correct answer due to the tendency of genera to predominate in emitting or non-emitting
339 species (Taylor et al., 2018). All species for which no emission data were available at the
340 genus level were excluded from the analyses. The imputed isoprene emission status and
341 associated information for each of our study species can be found in Table S2. The source
342 data (literature reference or present study metadata) for each species that informed the
343 imputation can be found in Table S3.
344

345 *2.9 Modeled isoprene flux estimates - Model of Emissions of Gases and Aerosols from* 346 *Nature (MEGAN)*

347
348 Isoprene fluxes were simulated using the MEGAN version 2.1 model in which the flux
349 activity factor for isoprene (γ_i) is proportional to the emission response to light (γ_P),
350 temperature (γ_T), leaf age (γ_A), soil moisture (γ_{SM}), leaf area index (LAI), and CO_2
351 inhibition (γ_{CO_2}) according to Eq. (2) (Guenther et al., 2012):

$$352 \quad \gamma_i = C_{CE} LAI \gamma_P \gamma_T \gamma_A \gamma_{SM} \gamma_{CO_2} \quad (2)$$

353
354
355 For this study, the canopy environment model of Guenther et al. (2006) was used with a
356 canopy environment coefficient (C_{CE}) of 0.57. MEGAN was run accounting for variations
357 in light, temperature, and LAI fractionated into leaf age classes. CO_2 inhibition and soil
358 moisture activity factors were set equal to a constant of 1, assuming these parameters do
359 not vary. For all simulations, we assumed no seasonal variation in soil moisture because
360 the soil moisture observed in this site consistently exceeds the threshold for the isoprene
361 drought response in MEGAN 2.1 (Guenther et al., 2012), which means that MEGAN would
362 predict no variation in isoprene emission resulting from the observed changes in soil
363 moisture (Fig. 1).
364



365 Solar radiation (PPFD) and air temperature inputs for all model simulations were obtained
366 from measurements at the INSTANT tower. Air temperature at 36 m height above ground
367 level was measured with a temperature and relative humidity sensor (CS215-L, Campbell Scientific
368 Inc., Logan, Utah, USA). In cases where the air temperature measurement at 36 m height failed,
369 the missing data were gap-filled with air temperature data available at other heights (73 m, 55 m,
370 40 m, 12 m), measured with CS215-L sensors installed on the INSTANT tower, or with the air
371 temperature at 18 m above the ground measured with a thermocouple (Conatex, St. Wendel,
372 Germany), installed along one evergreen tree of the species *Buchenavia parvifolia* (Combretaceae),
373 located 95 m away from the INSTANT tower. In cases where all the air temperature sensors failed
374 for less than 4 hours, the missing air temperature at 36 m height was gap-filled by linear
375 interpolation, visually checking data quality. In cases where no air temperature measurement was
376 available for a long time (e.g., one day, 2 months etc.), confirmed several times in 2013, the missing
377 air temperature at 36 m height was gap-filled by a multiple regression model developed with three
378 predictor variables: half-hourly variation of the soil temperature at 10 cm depth, soil heat flux, and
379 volumetric soil water content at 40 cm depth. The model training period was from 2013 June to
380 2014 May because the three predictor variables were usually available through the one-year period.
381 The developed model was validated based on the observation dataset from June 2014 to May 2015,
382 which showed good agreement with observed air temperature data at 36 m height during the
383 validation period ($R^2 = 0.83$; RMSE = 1.21; $n = 7473$). The developed and validated model was
384 applied to the three predictor variables measured in 2013 for gap-filling the long-term missing data
385 of air temperature at 36 m height. In cases where the predictor variables were unavailable in 2013,
386 the missing data were gap-filled using Akima interpolation with visual data quality checks.
387 Incoming and outgoing shortwave radiation was measured with a net radiometer (NR- Lite2, Kipp
388 & Zonen, the Netherlands) at 75 m above ground. In cases where the radiation measurement failed
389 for no more than 1 hour, the missing radiation data were gap-filled by linear interpolation, visually
390 checking data quality. In cases where radiation data were unavailable for more than 1 hour, the
391 missing data were gap-filled by the mean diurnal course (over ± 15 -day) method. Lastly, we used
392 a constant value (5.32) for the LAI and normalized it with monthly leaf age fractions
393 obtained from the phenocam observations to derive the canopy leaf age for each month
394 (see section 2.6). More details on model settings are found in Guenther et al. (2012).

395

396 **3. Results and Discussion**

397

398 *3.1 Observations of canopy isoprene mixing ratios*

399

400 We observed intra- and inter-annual variability of isoprene mixing ratios in canopy profiles
401 from nine intensive campaigns from Nov 2012 to Oct 2015 (Fig. 2a and Table 1). Figure
402 2b shows the leaf area density profile measured around the INSTANT tower in Oct 2015
403 and the mean canopy height. In general, isoprene mixing ratios were higher during the dry-
404 to-wet transition season (Nov 2012) and the dry season (Aug 2014 and Oct 2015/El-niño
405 year) than the wet season (Feb and Mar in 2013 and 2014) and the wet-to-dry transition
406 season (Jun 2013); with an exception for the Sep 2013-dry season that showed values
407 comparable to the 2014-wet season, although still higher than the 2013-wet season.
408 Interestingly, mean isoprene mixing ratios in Oct 2015 (El-niño dry season) were slightly
409 higher than those observed in Aug 2014 and Sep 2013 (both dry seasons) but not higher
410 than those observed in Nov 2012 (dry-to-wet transition) (although this was variable and
411 not significant). Seasonal changes in isoprene mixing ratios and fluxes from central
412 Amazonia have already been reported and were related to variations in temperature, light

413 availability at the surface, and leaf phenology (Yáñez-Serrano et al., 2015; Alves et al.,
414 2016, 2018; Wei et al., 2018; Langford et al., 2022), but the assessment of inter-annual
415 variability of consecutive years including anomalous years was lacking. Considering the
416 increased air temperatures observed in the 2015-El-niño dry season (Fig. 1b) and the fact
417 that tropical plant species emit high amounts of isoprene at high temperatures (Harley et
418 al., 2004; Alves et al., 2014; Jardine et al., 2014, Garcia et al., 2019; Rodrigues et al., 2020),
419 one could expect considerably higher emission and thereby high air mixing ratios of
420 isoprene during this extreme year. However, the 2015-El-niño dry season might have been
421 stressful for plants, with the anomalous drought (see soil moisture reduction in Fig. 1 d)
422 likely offsetting the high-temperature stimulus on isoprene emission. This finding can be
423 supported by two studies performed on this study site. Firstly, isoprene emission measured
424 in hyperdominant tree species showed a reduction in emission from the wet to the dry
425 season with a compensating increase in emission of monoterpenes and sesquiterpenes that
426 have both temperature-dependent emissions, indicating that the reduction in isoprene
427 emission and the shift toward heavier compounds resulted from abiotic stresses (e.g.,
428 drought) during the dry season (Gomes Alves et al., 2022), which might be substantially
429 higher in an extreme El-niño year. Secondly, the anomalous post-drought leaf flush
430 observed in Feb-Mar 2016 suggested that trees flushed out new leaves to recover from the
431 stress suffered during the 2015-El-niño dry season (Gonçalves et al., 2020).

432
433 Another interesting result was the seasonal variation in the shape of the isoprene mixing
434 ratio profiles (Fig. 2a). In general, all wet seasons (Feb-Mar 2013/2014) and the wet-to-dry
435 transition season (Jun 2013) data showed a constant profile with no clear vertical gradient
436 of isoprene. On the other hand, the dry seasons (Sep 2013, Aug 2014, and Oct 2015)
437 showed maximum mixing ratios between 12 m and 24m, and the dry-to-wet transition
438 season (Nov 2012) presented a well-defined peak at 24 m. This variation in the shape of
439 the isoprene mixing ratio profiles could result from a combination of variations in the
440 canopy leaf area density profile and canopy leaf age distribution throughout the year. The
441 total amount of LAI has a small variation over the year; still, the fractions of leaf ages that
442 compose this total LAI changes seasonally (Wu et al., 2016), as well as the shape of the
443 canopy leaf area density profile, with significant changes at the upper canopy (Martins
444 Rosa, 2016). During the wet-to-dry transition season (May-Jun) and the dry season (Jul-
445 Oct), upper canopy trees presented leaf abscission and leaf flushing (Lopes et al., 2016,
446 Gonçalves et al., 2020), and the maturing process on the following months toward the
447 beginning of the wet season (Nov-Jan) might translate into higher leaf area density at the
448 upper canopy (Martins Rosa, 2016) and higher gross primary productivity (GPP) fluxes
449 (Botía et al., 2022). This implies that two processes might be simultaneously occurring:
450 one is that when there are more leaves at the upper canopy, less light penetrates the canopy,
451 which might induce the maximum isoprene emission at the upper canopy as observed in
452 Nov 2012; the other one is that leaves at the upper canopy can have higher photosynthesis
453 rates and, consequently, a higher isoprene emission factor when they are mature (Alves et
454 al., 2014), and more mature leaves and higher GPP were observed in this study site during
455 the dry-to-wet transition season and beginning of the wet season (Lopes et al., 2016;
456 Gonçalves et al., 2020; Botía et al., 2022).

457

458 In addition, it has been suggested that seasonal variations in isoprene emissions could result
459 from a variation in the isoprene emission factor with leaf aging, but there were not enough
460 observational studies to support it in the Amazon (Alves et al., 2018). Therefore, in the
461 next section, we show for the first time in-situ observations of isoprene emission factor at
462 leaf-level with known leaf age and infer how this, together with variation in canopy leaf
463 age distribution, likely affected intra- and inter-annual variability in emission during
464 sequenced years.

465

466 3.2 Seasonal changes in the isoprene emission factor (E_s)

467

468 The isoprene emission factor (E_s ; parameter measured at $1000 \mu\text{mol m}^{-2} \text{s}^{-1}$ PAR, 30°C) of
469 an ecosystem is determined by the fraction of species that emits this compound and by
470 variations in the E_s magnitude within species. Such variations may be conditioned by leaf
471 ontogenetic status (e.g., young leaves have no or low emission, and old leaves emit less
472 isoprene than mature leaves) and environment (e.g., sun-leaves have higher E_s than shade-
473 leaves) (Niinemets, 2016). We performed measurements of E_s from sun-adapted leaves
474 across different ages in 21 trees (from 20 tree species) located at the upper canopy and
475 around the tower, and values ranged from 0 to $3.52 \text{ mg m}^{-2} \text{ h}^{-1}$ (see all species and emission
476 values in table S1). Of these 21 trees, 60 % had isoprene emission detectable by our
477 analytical system (TD-GC-TOFMS), while the other 40% did not. To evaluate whether
478 the E_s changes with leaf aging, we calculated the E_s ratios of mature (3–6 months) to young
479 (0–1 month), growing (1–2 months), and old (>6 months) leaves within the same tree
480 individual. We observed that, for some trees, E_s can be reduced by half when leaves are
481 older than six months (Fig. 3 and table S1), but the average of all trees combined showed
482 a statistically significant E_s reduction of 36% in old leaves compared to mature leaves
483 (paired t-test, p-value <0.05).

484

485 As tropical species represent a mix of phenotypes with the predominance of non-deciduous
486 plants, it was impossible to sample all leaf age classes for all tree species measured.
487 Nevertheless, our dataset covers leaf ages from 15 to 578 days (table S1), and we observed
488 that all leaves measured at the young leaf age class did not show detectable isoprene
489 emission, and two leaves measured at the growing leaf age class showed emissions similar
490 to the mature leaf age class (Fig.3 and table S1). As our sampling did not cover a broad
491 range of leaf ages below 60 days, especially among isoprene emitters, to improve the
492 robustness of our analysis, we added another species that had the E_s measured from the leaf
493 flushing day until the 30th day (young class) and at 226-227 days (old class) in the
494 southwestern Amazonia (Kuhn et al., 2004b). With this tree species added, we calculated
495 that the emission activity of E_s of young (0–1 month) and old (>6 months) leaves were,
496 respectively, 1% and 64% of the E_s observed in growing (1–2 months) and mature leaves
497 (3–6 months) (paired t-test, p-value <0.05), and that there was no statistically significant
498 difference between growing and mature leaves (paired t-test, p-value >0.05) (Fig. 3 and
499 table S1).

500

501 Furthermore, we observed that emitter species from our dataset could be combined into
502 two qualitative emission categories – medium emitter and low emitter –, given their E_s
503 magnitude compared to other leaf-level measurements in Amazonia (see a detailed

504 compilation in Yañez-Serrano et al., 2020), and high emitter, with the data from the tree
505 species measured in southwestern Amazonia (Kuhn et al., 2004b) (Fig. 3). The maximum
506 E_s occurred in different leaf ages for each emitter category. Still, both high and medium
507 emitters had an E_s maximum before 150 days (mature). In contrast, the low emitter category
508 showed an E_s maximum in 295 days (old) for one species, but that was not statistically
509 significant when compared to all low emitter species (paired t-test, p-value >0.05).
510 Therefore, this indicates that species that emit considerable amounts of isoprene have
511 maximum E_s when their leaves are mature.

512
513 The variation of E_s across leaf ages is already known, also for tropical tree species (Kuhn
514 et al., 2004b; Alves et al., 2014); however, the quantification of these variations across
515 different species is still a challenge given the high biodiversity in the Amazonian rainforest,
516 and, although our results show the variation of E_s across leaf ages for more species than
517 previously reported, it is still necessary to further develop tools to upscale these results to
518 the ecosystem level. Earlier studies indicated that the capacity to emit isoprene is more
519 common, and the E_s magnitudes are expected to be the highest in deciduous tree species
520 (Harrison et al., 2013; Dani et al., 2014). In fact, the high emitter (Fig. 3) is a tropical
521 deciduous tree species with a large range of variation in E_s within 30 days after leaf flushing
522 and with the maximum E_s observed in mature leaves at the end of the dry season (Kuhn
523 et al., 2004b). However, the number of deciduous trees that have regular leaf abscission and
524 leaf flushing during the dry season in central Amazonia may represent less than 15% of the
525 whole tree assembly (Gonçalves et al., 2020), which means that the effect of high
526 variability in the E_s with leaf aging from those trees might be low at the ecosystem level,
527 especially when we compare it with the other trees that showed less variability in the E_s
528 (Fig. 3, table S1).

529
530 Furthermore, for Amazonian tree species, the categorization of phenological habits goes
531 beyond evergreen and deciduous. Here, with a dataset of 194 trees (Fig. 4, and table S2)
532 monitored with a phenocam for leaf phenology and demography from 2013 to 2018, we
533 derived: (i) the camera-based canopy leaf area index (LAI) fractionated into four leaf age
534 classes - young (≤ 1 month), growing (1-2 months), mature (3-6 months), and old (> 6
535 months) (Fig. 4a); and (ii) four classes of phenology (phenotypes) - evergreen, semi-
536 evergreen, brevi-deciduous, and semi-brevideciduous (Fig. 4c), based on the frequency of
537 events of leaf abscission and leaf flushing (more details in Supplementary Information).
538 Then, we assigned the isoprene trait for these tree species with measurements and literature
539 data, and imputed the trait to non-measured species by following the method described in
540 Taylor et al. (2018) (Fig. 4 c). We observed that the isoprene trait did not have a higher
541 percentage within brevi-deciduous and semi-brevideciduous phenotypes, which have
542 regular and seasonal leaf abscission and leaf flushing. Instead, all phenotypes had a similar
543 fraction of isoprene emitters (Fig. 4c). This implies that leaf age is an important factor for
544 the magnitude of E_s regardless of phenotype.

545
546 Although we do not have enough data to infer the phenotypes for the species monitored at
547 the branch level, we observed that the leaf age distribution of the 36 trees (Fig. 4b) was
548 similar to the 194 trees monitored with the phenocam (Fig. 4a); and that the fraction of
549 isoprene emitters was also similar when measured (21 trees – 60% emitters; Fig. 3) and
550 non-measured (15 trees – 47% emitters) were combined (56% emitters) (Fig. 4d) and

551 compared to the phenocam trees (60% emitters) (Fig. 4c). Note that the tree species that
552 had no isoprene emission trait reported in the literature and did not fill the assumptions
553 necessary to input the trait, according to Taylor et al. (2018), were assigned with the
554 unknown flag (NA).

555
556 The similarity found in the seasonal leaf age distribution between the 194 trees monitored
557 by the phenocam and the 36 trees monitored at the branch level (Fig. 4) is in agreement
558 with the results presented by Gonçalves et al. (2020), which showed that the leaf phenology
559 and demography of the 194 trees are representative of the region of this study, by
560 comparing it to corresponding satellite vegetation indices retrieved from MODIS-MAIAC
561 (Multi-Angle Implementation of Atmospheric Correction). Also, this, together with the fact
562 that the isoprene trait distribution was similar among the scales (leaf level and upper
563 canopy), implies that the E_s variation with leaf age measured here can be used to optimize
564 model estimates for intra- and inter-annual isoprene emission.

565 566 *3.3 Modeling of isoprene emission*

567
568 We used MEGAN to estimate isoprene emissions for the periods that we have in-situ
569 observations of isoprene and model inputs without considerable gaps, i.e., the years 2014
570 and 2015. We performed four different simulations (Fig. 5 and Table 2). For our first
571 simulation (S1), we applied MEGAN default settings for tropical vegetation (Fig. 5c,d),
572 which means that we used the E_s assigned to the broadleaf evergreen tropical tree and the
573 broadleaf deciduous tropical tree that is equal to $7 \text{ mg m}^{-2} \text{ h}^{-1}$ (Guenther et al., 2012), half-
574 hourly averages of air temperature and PPFD data measured at the same tower as the
575 isoprene observations (Fig. 5a,b), and no change in the leaf age algorithm. For the second
576 simulation (S2), we used a modified leaf age algorithm by adding the monthly distribution
577 of the LAI fractionated into leaf age classes (young, growing, mature, and old) as described
578 in the section above (Fig. 5c,d).

579
580 For a direct comparison between observations and model simulations, we performed eddy
581 covariance (EC) isoprene flux measurements during 11 days during Nov 2015 and
582 compared them with the simulations (Fig. 6). The isoprene emission sensitivity to the PPFD
583 circadian cycle was well simulated by MEGAN when estimates were compared with EC
584 isoprene flux ($r^2=0.84$, p -value <0.01) (Fig. 6 g). However, MEGAN simulations (S1 and
585 S2) overestimated the magnitude of emissions when compared with EC isoprene flux
586 around noontime (Fig. 6b); S1 and S2 had a daily average flux 2.71 and 2.68 times higher
587 than EC isoprene flux ($p<0.01$), respectively (Fig. 6h). This overestimation was a result of
588 a high value for E_s in the model setup ($7 \text{ mg m}^{-2} \text{ h}^{-1}$). To support this finding, we calculated
589 E_s from the observed EC isoprene flux data from 06:00 to 18:00 with the G93 algorithm
590 (Guenther et al., 1993), and E_s resulted in $3.21 \pm 1.76 \text{ mg m}^{-2} \text{ h}^{-1}$. We then ran a third
591 simulation (S3) with the corrected E_s ($3.21 \text{ mg m}^{-2} \text{ h}^{-1}$) (Fig. 5c,d; Fig. 6b) and S3 estimates
592 presented a daily average flux 1.23 higher than EC isoprene flux ($p=0.013$) (Fig. 6b,h). The
593 mean E_s calculated from EC isoprene flux is in the same range as the E_s observed for the
594 leaf level emissions of 21 trees (Fig. 3 and table S1), indicating that E_s from this study site
595 is lower than the one set in the model default.

596

597 Another modification in the model was done based on our leaf-level measurements. In
598 section 3.2, we present the E_s variation across leaf ages and suggest that the seasonal
599 variation in canopy leaf age distribution results in an emergent property to canopy seasonal
600 variation in E_s . With the LAI fractionated into leaf age classes (phenocam data) along the
601 year and the ratios of E_s (leaf level measurements) between mature and young leaves,
602 mature and old leaves, and mature and growing leaves, we modified the leaf age emission
603 activity factor of the leaf age algorithm in MEGAN. The modified leaf age emission
604 activity factor accounts for lower values of E_s in young and old leaves compared to mature
605 and growing leaves (Table 2). In our fourth simulation (S4) (Fig. 5c,d; Fig. 6b), we added
606 the modification in the leaf age emission activity factor, which led to a daily average 1.15
607 higher than EC isoprene flux ($p=0.03$) (Fig. 6 h).
608

609 To evaluate the effectiveness of our modifications in the model on intra- and inter-annual
610 timescales, we compared the isoprene mixing ratios observed at 38m height in all
611 campaigns performed in 2014 and 2015 with the four simulations. As our observations,
612 except for Nov 2015, are mixing ratios, it is only possible to indirectly compare with
613 MEGAN using an atmospheric model. However, considering that isoprene emission is
614 primarily driven by changes in light, temperature, and leaf phenology (Alves et al., 2018)
615 and that the variability of these factors was included in the model, we can still test the
616 comparability of the changes in the magnitudes from our measurements and simulations
617 that resulted from intra- and inter-annual variations. In figure 7, we show linear regressions
618 between observations and simulations. All datasets were filtered to the period between 12-
619 15h, local time, to evaluate the time of the day with maximum emission and high mixing
620 in the surface layer and to reduce variability in photochemical isoprene loss rates. Figure
621 7a shows daily hourly averages (12-15h, local time) of observed mixing ratios and the four
622 simulations for isoprene from Feb and Mar 2014, Aug 2014, and Oct 2015, and, apart from
623 the slope, all simulations were similarly and significantly comparable to observations
624 ($r^2=0.41$ and $r^2=0.42$, $p \ll 0.01$). As significant day-to-day isoprene variability was
625 observed - also over other Amazon regions, with isoprene concentrations of similar
626 magnitudes occurring during both wet and dry seasons, likely resulting from the longer wet
627 season lifetimes of isoprene (Wells et al., 2022) - we averaged our datasets for each month
628 that we have observations and simulations. Figure 7b shows the monthly averages (12-15h,
629 local time) of mixing ratios and emission estimates for isoprene. We observed that our
630 modifications in the model improved the estimates (from $r^2=0.76$ to $r^2=0.83$). However, the
631 differences were less significant ($p=0.08$) compared to the linear regression with daily
632 hourly averages ($p \ll 0.01$) (Fig. 7a). We expect that if more isoprene flux data, especially
633 from long-term measurements, were available for comparison with our simulations, we
634 could have more significant results.
635

636 In general, the modifications for the E_s (S3 and S4) and the leaf age activity factor (S4)
637 improved the estimates because they account for biological factors that have intra- and
638 inter-annual variations in this study site (Gonçalves et al., 2020), which represent a major
639 source of uncertainty in MEGAN (Niinemets et al., 2010). In this light, the main
640 improvement presented here resulted from the E_s correction since our observations showed
641 that E_s was less than half of the value in the model default settings and that E_s varies
642 significantly among leaf ages. This is important because E_s is a crucial factor in determining

643 the magnitudes of emission of a specific site, which may vary substantially in Amazonia.
644 Although a long-term canopy flux measurement study in central Amazonia indicated that
645 E_s does not vary seasonally and argued that intra-annual changes in isoprene emission
646 resulted only from micrometeorological and LAI variations (Langford et al., 2022), other
647 studies in central Amazonia have shown that emission varies substantially in a relatively
648 small spatial scale and on topographic gradients (Gu et al., 2017; Batista et al., 2019); and,
649 more recently, leaf-level measurements have shown that E_s varies within tree species both
650 seasonally and spatially, in particular when these species occur in different forest types and
651 topography (Gomes Alves et al., 2022).

652

653 *3.4 Implications of intra- and inter-annual variabilities in isoprene emission for modeling*

654

655 Despite the high variability within seasons, our results showed significant changes between
656 seasons. We corroborate previous studies indicating that intra-annual variability in isoprene
657 emission results from changes in solar radiation, temperature, and leaf phenology (e.g.,
658 Yáñez-Serrano et al., 2015; Alves et al., 2016, 2018), but we suggest that there is seasonal
659 variation in the ecosystem E_s resulting from changes in canopy leaf age distribution and
660 that this may contribute to the seasonality in the magnitude of actual emission rates. Even
661 though we only derived the ecosystem E_s from canopy isoprene flux measured in Nov 2015
662 - an El-niño year, when we compared the ecosystem E_s to the values from leaves measured
663 in Oct-Nov 2017 (normal year), we observed both were in the same range. It is important
664 to note that leaf-level E_s from Oct-Nov 2017 showed significant differences among leaf
665 ages, with maximum values for mature leaves, and those values were similar to the
666 ecosystem E_s measured in Nov 2015. Nonetheless, it is also worth noting that Oct and Nov
667 (dry season and dry-to-wet transition seasons) are months with a substantially higher
668 fraction of mature leaves in the canopy compared to those from the wet and wet-to-dry-
669 transition seasons, meaning that the E_s from mature leaves likely predominates the
670 ecosystem E_s in Oct-Nov. In this sense, we suggest that understanding how the E_s changes
671 over seasons due to leaf age composition within LAI will considerably improve model
672 estimates of intra-annual variations in isoprene. However, more long-term measurements
673 of canopy isoprene flux are needed to test it.

674

675 Surprisingly, inter-annual variabilities were less pronounced than intra-annual variability
676 when comparing normal years with the 2015-El-niño year. Our air temperature
677 measurements showed a significant increase during the dry season of 2015-El-niño year
678 compared to normal years. On a larger scale, regional land surface temperature retrieved
679 by satellite showed an increase of up to + 4 °C from Oct to Dec 2015 in the Amazon basin
680 (Jiménez-Muñoz et al., 2016), and that was accompanied by a significant negative
681 maximum climatological water deficit in 43% of the whole Amazon rainforest (Aragão et
682 al., 2018). Such stresses were expected to provide a stimulus for isoprene emission, as it
683 is already largely known that isoprene emission can increase with increasing temperature and
684 that some studies have also shown that emissions increase after moderate drought (e.g.,
685 Werner et al., 2021). However, our results did not show a significant increase in isoprene
686 mixing ratios in Oct 2015 compared to the dry seasons of previous years. Understanding
687 mechanisms of intra- and inter-annual variations in canopy emissions of isoprene is
688 essential for predicting their influence on atmospheric chemical-physical processes. For

689 example, the contribution of isoprene as a sink for hydroxyl radical (OH) varied seasonally
690 (Nölscher et al., 2016); however, it did not vary significantly when a normal year and the
691 2015-El-niño year were compared in this study site (Pfannerstill et al., 2018), leading to
692 the conclusion that these forests contributed to the emission of other compounds to cope
693 with the stress during the 2015-El-niño year, resulting in an effect on the atmospheric
694 oxidative capacity (Pfannerstill et al., 2021).

695
696 Some models predicted that higher temperatures and extended drought periods resulting
697 from climate change might increase global isoprene emissions (Pegoraro et al., 2006).
698 However, more recently, a synthesis of studies performed in the Amazon suggested that,
699 as the increase in temperature comes along with biomass loss given deforestation and forest
700 degradation, a decrease in isoprene emission from Amazonia may be expected (Yáñez-
701 Serrano et al., 2020). Interestingly, although isoprene emission was not considerably higher
702 in the dry season of the 2015-El-niño year, previous studies observed higher monoterpene
703 emissions compared to other dry seasons (Yáñez-Serrano et al., 2018) and even higher
704 monoterpene emissions in drier and warmer days of the 2015-El-niño dry season
705 (Pfannerstill et al., 2018). In addition, another study conducted in central Amazonia
706 reported that the heat in 2015/16 led to a shift in plant emissions to more reactive
707 monoterpenes such as β -ocimene and that at high temperatures, monoterpene emissions
708 can be decoupled from photosynthesis (Jardine et al., 2017). Recently, leaf-level E_s
709 measurements in hyperdominant tree species in this study site showed that photosynthesis
710 and isoprene decreased while monoterpenes and sesquiterpenes proportionally increased
711 in the dry season, suggesting that plants might have emitted heavier compounds to cope
712 with the stress caused by high temperatures and potentially drought (Gomes Alves et al.,
713 2022). We suggest that anomalies in isoprene emission during extreme years are less
714 expected than anomalies in emissions of monoterpenes and sesquiterpenes since plants may
715 also emit compounds from their storage pools when there is a limited carbon supply to
716 produce isoprene, as might be the case of plants reducing photosynthesis under heat and
717 drought stresses.

718

719 **Summary and conclusions**

720

721 Understanding mechanisms of intra- and inter-annual variations in canopy emissions of
722 isoprene from Amazonia is essential for predicting their influence on atmospheric
723 chemical-physical processes, especially when considering the role of Amazonia in the
724 global BVOC emission budget. Earlier studies presented seasonal isoprene emissions and
725 related them to the seasonality of temperature, solar radiation, and leaf phenology.
726 Nevertheless, to the best of our knowledge, this is the first study showing the E_s variation
727 across leaf ages for several Amazonian tree species and the first attempt to represent the
728 effect on seasonal isoprene flux with a model parameterization. Also, by comparing
729 observations of normal years to the extreme 2015-El-niño year, we were able to show that
730 isoprene emission does not substantially increase as a result of higher temperatures. We
731 suggest that the stress caused by elevated temperatures and droughts in extreme years might
732 reduce the isoprene temperature dependence, which is not currently well represented in
733 modeling.

734 Even though there are uncertainties related to measurements and model simulations, the
735 results presented here suggest that E_s varied seasonally and that this is a key factor in
736 improving model predictions. Additionally, previous studies showed that a distinguished
737 high monoterpene emission accompanies a non-pronounced increase in isoprene emission
738 in extreme years during the dry season at this study site, which is interesting to investigate
739 further since monoterpenes have higher reactivity in the atmosphere. Therefore, more
740 detailed and long-term measurements of isoprene and other BVOCs are encouraged to
741 improve our understanding of the intra- and inter-annual variability of BVOC emissions in
742 Amazonia, especially measurements that also account for biological factors that might
743 contribute to more mechanistic surface emission modeling and subsequently lead to better
744 predictions of atmospheric chemical-physical processes.

745

746 **Data availability**

747 Datasets are available upon request on <https://attodata.org>.

748

749 **Authors' contributions**

750 Eliane Gomes Alves has designed this study and performed the leaf-level measurements,
751 the statistical analysis of observational datasets, and the MEGAN simulations. Raoni
752 Santana and Cleo Quaresma have contributed to the analysis of the datasets of canopy
753 isoprene mixing ratios and of micrometeorology. Santiago Botía has contributed to the
754 analysis of the phenocam dataset and performed the MEGAN simulations. Tyeen Taylor
755 contributed new measurements of isoprene emissions from tropical tree species and the
756 imputation modeling of isoprene trait to the tree species monitored by the phenocam. Ana
757 Maria Yáñez-Serrano and Jürgen Kesselmeier have provided the canopy isoprene mixing
758 ratios dataset. Pedro Ivo Lembo Silveira de Assis and Giordane Martins have contributed
759 with the leaf age monitoring at the branch level. Rodrigo de Souza and Sergio Duvoisin
760 Junior contributed to the collection of isoprene samples measured at leaf-level. Alex
761 Guenther and Dasa Gu have contributed with the chemical analysis of isoprene samples
762 measured at leaf-level and the MEGAN simulations. Anywhere Tsokankunku and Matthias
763 Sörgel contributed with the dataset of eddy covariance isoprene flux. Bruce Nelson and
764 Davieliton Pinto contributed to the collection and the analysis of the phenocam dataset.
765 Shujiro Komiya contributed to analyzing the micrometeorology dataset to run the MEGAN
766 simulations. Diogo Martins contributed to the surface LiDAR data collection and analysis.
767 Bettina Weber and Cybelli Barbosa contributed with the temperature dataset to run the
768 MEGAN simulations. Michelle Robin contributed new measurements of isoprene
769 emissions from tropical tree species. Kenneth Feeley, Alvaro Duque, Viviana Lemos,
770 Maria Contreras, Alvaro Idarraga, Norberto Lopez, Chad Husby, and Brett Jestrow
771 contributed expert guidance, specimen curation, field assistance, and botanical
772 identifications for isoprene measurements from trees in botanic gardens and private
773 collections. All authors contributed to the writing of the manuscript.

774

775 **Competing interests**

776 The authors declare that they have no conflict of interest

777

778

779

780 **Acknowledgements**

781 We thank the National Institute of Amazonian Research (INPA) and the Max Planck
782 Institute for Biogeochemistry (MPI-BGC) for their continuous support. We acknowledge
783 the support by the ATTO project (German Federal Ministry of Education and Research,
784 BMBF funds 01LB1001A; Brazilian Ministry of Science, Technology, Innovation and
785 Communication; FINEP/MCTIC contract 01.11.01248.00); UEA and FAPEAM,
786 LBA/INPA and SDS/CEUC/RDS-Uatumã. TCT was supported by grant #NSF-PRFB-
787 1711997, and #NSF-1754163. We also truly thank Marta Sá and Paulo Ricardo Teixeira
788 for their work on checking the quality of the micrometeorology dataset and the INPA's
789 Microteorology Lab for providing the dataset. We acknowledge the helpful support for
790 isoprene measurements in botanic gardens by Santiago Madriñan of the Jardín Botánico
791 "Guillermo Piñeres", Ana María Benavides and Juan David Fernandes of the Jardín
792 Botánico de Medellín, Carl Lewis and Chad Husby of the Fairchild Botanic Garden, and
793 Patrick Griffith, Joanna Tucker Lima, and Michelle Barros of the Montgomery Botanical
794 Garden. We would like to especially thank the field assistants and all the people involved
795 in the logistic support of the ATTO project, who were all imperative for the development
796 of this study. We also thank all the indigenous communities that have been bravely
797 protecting the forest, and the riverside communities that have always helped us to do our
798 science. Without the “mateiros” we could never accomplish our scientific goals.
799

800 **References**

801 Alves, E. G., Harley, P., Gonçalves, J. F. C., Moura, C. E. S., and Jardine, K.: Effects of
802 light and temperature on isoprene emission at different leaf developmental stages of
803 *eschweilera coriacea* in central amazon | efeitos da luz e da temperatura sobre a emissão de
804 isopreno em diferentes estádios de desenvolvimento foliar de *eschwe*, *Acta Amazon*, 44,
805 9–18, <https://doi.org/10.1590/S0044-59672014000100002>, 2014.
806 Alves, E. G., Jardine, K., Tota, J., Jardine, A., Yáñez-Serrano, A. M., Karl, T., Tavares, J.,
807 Nelson, B., Gu, D., Stavrou, T., Martin, S., Artaxo, P., Manzi, A., and Guenther, A.:
808 Seasonality of isoprenoid emissions from a primary rainforest in central Amazonia, *Atmos*
809 *Chem Phys*, 16, 3903–3925, <https://doi.org/10.5194/acp-16-3903-2016>, 2016.
810 Alves, E. G., Tóta, J., Turnipseed, A., Guenther, A. B., Vega Bustillos, J. O. W., Santana,
811 R. A., Cirino, G. G., Tavares, J. v., Lopes, A. P., Nelson, B. W., de Souza, R. A., Gu, D.,
812 Stavrou, T., Adams, D. K., Wu, J., Saleska, S., and Manzi, A. O.: Leaf phenology as one
813 important driver of seasonal changes in isoprene emissions in central Amazonia,
814 *Biogeosciences*, 15, 4019–4032, <https://doi.org/10.5194/bg-15-4019-2018>, 2018.
815 Andreae, M. O., Acevedo, O. C., Araújo, A., Artaxo, P., Barbosa, C. G. G., Barbosa, H.
816 M. J., Brito, J., Carbone, S., Chi, X., Cintra, B. B. L., da Silva, N. F., Dias, N. L., Dias-
817 Júnior, C. Q., Ditas, F., Ditz, R., Godoi, A. F. L., Godoi, R. H. M., Heimann, M., Hoffmann,
818 T., Kesselmeier, J., Könemann, T., Krüger, M. L., Lavric, J. v., Manzi, A. O., Lopes, A.
819 P., Martins, D. L., Mikhailov, E. F., Moran-Zuloaga, D., Nelson, B. W., Nölscher, A. C.,
820 Santos Nogueira, D., Piedade, M. T. F., Pöhlker, C., Pöschl, U., Quesada, C. A., Rizzo, L.
821 v., Ro, C. U., Ruckteschler, N., Sá, L. D. A., de Oliveira Sá, M., Sales, C. B., dos Santos,
822 R. M. N., Saturno, J., Schöngart, J., Sörgel, M., de Souza, C. M., de Souza, R. A. F., Su,
823 H., Targhetta, N., Tóta, J., Trebs, I., Trumbore, S., van Eijck, A., Walter, D., Wang, Z.,
824 Weber, B., Williams, J., Winderlich, J., Wittmann, F., Wolff, S., and Yáñez-Serrano, A.
825 M.: The Amazon Tall Tower Observatory (ATTO): Overview of pilot measurements on

- 826 ecosystem ecology, meteorology, trace gases, and aerosols, *Atmos Chem Phys*, 15, 10723–
827 10776, <https://doi.org/10.5194/acp-15-10723-2015>, 2015.
- 828 Aragão, L. E. O. C., Anderson, L. O., Fonseca, M. G., Rosan, T. M., Vedovato, L. B.,
829 Wagner, F. H., Silva, C. V. J., Silva Junior, C. H. L., Arai, E., Aguiar, A. P., Barlow, J.,
830 Berenguer, E., Deeter, M. N., Domingues, L. G., Gatti, L., Gloor, M., Malhi, Y., Marengo,
831 J. A., Miller, J. B., Phillips, O. L., and Saatchi, S.: 21st Century drought-related fires
832 counteract the decline of Amazon deforestation carbon emissions, *Nat Commun*, 9, 1–12,
833 <https://doi.org/10.1038/s41467-017-02771-y>, 2018.
- 834 Artaxo, P., Mohr, C., and Pöschl, U.: Tropical and Boreal Forest – Atmosphere
835 Interactions: A Review, 74, 24–163, <https://doi.org/https://doi.org/10.16993/tellusb.34>,
836 2022.
- 837 Atkinson, R.: Gas-Phase Tropospheric Chemistry of Volatile Organic Compounds: 1.
838 Alkanes and Alkenes, *J Phys Chem Ref Data*, 26, 215–290,
839 <https://doi.org/10.1063/1.556012>, 1997.
- 840 Barkley, M. P., Palmer, P. I., de Smedt, I., Karl, T., Guenther, A., and van Roozendaal, M.:
841 Regulated large-scale annual shutdown of Amazonian isoprene emissions?, *Geophys Res*
842 *Lett*, 36, L04803, <https://doi.org/10.1029/2008GL036843>, 2009.
- 843 Batista, C. E., Ye, J., Ribeiro, I. O., Guimarães, P. C., Medeiros, A. S. S., Barbosa, R. G.,
844 Oliveira, R. L., Duvoisin, S., Jardine, K. J., Gu, D., Guenther, A. B., McKinney, K. A.,
845 Martins, L. D., Souza, R. A. F., and Martin, S. T.: Intermediate-scale horizontal isoprene
846 concentrations in the near-canopy forest atmosphere and implications for emission
847 heterogeneity, *Proceedings of the National Academy of Sciences*, 116, 19318–19323,
848 <https://doi.org/10.1073/pnas.1904154116>, 2019.
- 849 Bauwens, M., Stavrou, T., Müller, J. F., de Smedt, I., van Roozendaal, M., van der Werf,
850 G. R., Wiedinmyer, C., Kaiser, J. W., Sindelarova, K., and Guenther, A.: Nine years of
851 global hydrocarbon emissions based on source inversion of OMI formaldehyde
852 observations, *Atmos Chem Phys*, 16, 10133–10158, [https://doi.org/10.5194/acp-16-10133-](https://doi.org/10.5194/acp-16-10133-2016)
853 2016, 2016.
- 854 Botía, S., Komiya, S., Marshall, J., Koch, T., Gałkowski, M., Lavric, J., Gomes-Alves, E.,
855 Walter, D., Fisch, G., Pinho, D. M., Nelson, B. W., Martins, G., Luijkx, I. T., Koren, G.,
856 Florentie, L., Carioca de Araújo, A., Sá, M., Andreae, M. O., Heimann, M., Peters, W., and
857 Gerbig, C.: The CO₂ record at the Amazon Tall Tower Observatory: A new opportunity
858 to study processes on seasonal and inter-annual scales, *Glob Chang Biol*, 28, 588–611,
859 <https://doi.org/10.1111/gcb.15905>, 2022.
- 860 Boulton, C. A., Lenton, T. M., and Boers, N.: Pronounced loss of Amazon rainforest
861 resilience since the early 2000s, *Nat Clim Chang*, 12, 271–278,
862 <https://doi.org/10.1038/s41558-022-01287-8>, 2022.
- 863 Boyle, B., Hopkins, N., Lu, Z., Raygoza Garay, J. A., Mozzherin, D., Rees, T., Matasci,
864 N., Narro, M. L., Piel, W. H., McKay, S. J., Lowry, S., Freeland, C., Peet, R. K., and
865 Enquist, B. J.: The taxonomic name resolution service: an online tool for automated
866 standardization of plant names, *BMC Bioinformatics*, 14, 16, [https://doi.org/10.1186/1471-](https://doi.org/10.1186/1471-2105-14-16)
867 2105-14-16, 2013.
- 868 Boyle, B. L., Matasci, N., Mozzherin, D., Rees, T., Barbosa, G. C., Kumar Sajja, R., &
869 Enquist, B. J. (2021). Taxonomic Name Resolution Service, version 5.0. In *Botanical*
870 *Information and Ecology Network*. <https://tnrs.biendata.org/>

- 871 Bracho-Nunez, A., Knothe, N. M., Welter, S., Staudt, M., Costa, W. R., Liberato, M. A.
872 R., Piedade, M. T. F., and Kesselmeier, J.: Leaf level emissions of volatile organic
873 compounds (VOC) from some Amazonian and Mediterranean plants, *Biogeosciences*, 10,
874 5855–5873, <https://doi.org/10.5194/bg-10-5855-2013>, 2013.
- 875 Canaval, E., Millet, D. B., Zimmer, I., Nosenko, T., Georgii, E., Partoll, E. M., Fischer, L.,
876 Alwe, H. D., Kulmala, M., Karl, T., Schnitzler, J., and Hansel, A.: Rapid conversion of
877 isoprene photooxidation products in terrestrial plants, *Commun Earth Environ*, 1, 44,
878 <https://doi.org/10.1038/s43247-020-00041-2>, 2020.
- 879 Dani, K. G. S., Jamie, I. M., Prentice, I. C., and Atwell, B. J.: Evolution of isoprene
880 emission capacity in plants, *Trends Plant Sci*, 19, 439–446,
881 <https://doi.org/10.1016/j.tplants.2014.01.009>, 2014.
- 882 Fauset, S., Johnson, M. O., Gloor, M., Baker, T. R., Monteagudo M., A., Brienen, R. J. W.,
883 Feldpausch, T. R., Lopez-Gonzalez, G., Malhi, Y., ter Steege, H., Pitman, N. C. A.,
884 Baraloto, C., Engel, J., Pétronelli, P., Andrade, A., Camargo, J. L. C., Laurance, S. G. W.,
885 Laurance, W. F., Chave, J., Allie, E., Vargas, P. N., Terborgh, J. W., Ruokolainen, K.,
886 Silveira, M., Aymard C., G. A., Arroyo, L., Bonal, D., Ramirez-Angulo, H., Araujo-
887 Murakami, A., Neill, D., Hérault, B., Dourdain, A., Torres-Lezama, A., Marimon, B. S.,
888 Salomão, R. P., Comiskey, J. A., Réjou-Méchain, M., Toledo, M., Licona, J. C., Alarcón,
889 A., Prieto, A., Rudas, A., van der Meer, P. J., Killeen, T. J., Marimon Junior, B. H., Poorter,
890 L., Boot, R. G. A., Stergios, B., Torre, E. V., Costa, F. R. C., Levis, C., Schiatti, J., Souza,
891 P., Groot, N., Arets, E., Moscoso, V. C., Castro, W., Coronado, E. N. H., Peña-Claros, M.,
892 Stahl, C., Barroso, J., Talbot, J., Vieira, I. C. G., van der Heijden, G., Thomas, R., Vos, V.
893 A., Almeida, E. C., Davila, E. Á., Aragão, L. E. O. C., Erwin, T. L., Morandi, P. S., de
894 Oliveira, E. A., Valadão, M. B. X., Zagt, R. J., van der Hout, P., Loayza, P. A., Pipoly, J.
895 J., Wang, O., Alexiades, M., Cerón, C. E., Huamantupa-Chuquimaco, I., di Fiore, A.,
896 Peacock, J., Camacho, N. C. P., Umetsu, R. K., de Camargo, P. B., Burnham, R. J., Herrera,
897 R., Quesada, C. A., Stropp, J., Vieira, S. A., Steininger, M., Rodríguez, C. R., Restrepo,
898 Z., Muelbert, A. E., Lewis, S. L., Pickavance, G. C., and Phillips, O. L.: Hyperdominance
899 in Amazonian forest carbon cycling, *Nat Commun*, 6, 1–9,
900 <https://doi.org/10.1038/ncomms7857>, 2015.
- 901 Fu, D., Millet, D. B., Wells, K. C., Payne, V. H., Yu, S., Guenther, A., and Eldering, A.:
902 Direct retrieval of isoprene from satellite-based infrared measurements, *Nat Commun*, 10,
903 3811, <https://doi.org/10.1038/s41467-019-11835-0>, 2019.
- 904 Garcia, S., Jardine, K., de Souza, V. F., de Souza, R. A. F., Junior, S. D., and Gonçalves,
905 J. F. de C.: Reassimilation of leaf internal CO₂ contributes to isoprene emission in the
906 neotropical species *inga edulis* Mart, *Forests*, 10, <https://doi.org/10.3390/f10060472>, 2019.
- 907 Geron, C., Guenther, A., Greenberg, J., Loeschner, H. W., Clark, D., and Baker, B.: Biogenic
908 volatile organic compound emissions from a lowland tropical wet forest in Costa Rica,
909 *Atmos Environ*, 36, 3793–3802, [https://doi.org/10.1016/S1352-2310\(02\)00301-1](https://doi.org/10.1016/S1352-2310(02)00301-1), 2002.
- 910 Gomes Alves, E., Taylor, T., Robin, M., Pinheiro Oliveira, D., Schiatti, J., Duvoisin Júnior,
911 S., Zannoni, N., Williams, J., Hartmann, C., Gonçalves, J. F. C., Schöngart, J., Wittmann,
912 F., and Piedade, M. T. F.: Seasonal shifts in isoprenoid emission composition from three
913 hyperdominant tree species in central Amazonia, *Plant Biol*, 24, 721–733,
914 <https://doi.org/10.1111/plb.13419>, 2022.
- 915 Gonçalves, N., Pontes, A., Dalagnol, R., Wu, J., Mesquita, D., and Walker, B.: Remote
916 Sensing of Environment Both near-surface and satellite remote sensing confirm drought

- 917 legacy effect on tropical forest leaf phenology after 2015 / 2016 ENSO drought, *Remote*
918 *Sens Environ*, 237, 111489, <https://doi.org/10.1016/j.rse.2019.111489>, 2020.
- 919 Gu, D., Guenther, A. B., Shilling, J. E., Yu, H., Huang, M., Zhao, C., Yang, Q., Martin, S.
920 T., Artaxo, P., Kim, S., Seco, R., Stavrou, T., Longo, K. M., Tóta, J., de Souza, R. A. F.,
921 Vega, O., Liu, Y., Shrivastava, M., Alves, E. G., Santos, F. C., Leng, G., and Hu, Z.:
922 Airborne observations reveal elevational gradient in tropical forest isoprene emissions, *Nat*
923 *Commun*, 8, <https://doi.org/10.1038/ncomms15541>, 2017.
- 924 Guenther, A., Nicholas, C., Fall, R., Klinger, L., Mckay, W. A., and Scholes, B.: A global
925 model of natural volatile organic compound emissions s Raja the balance Triangle changes
926 in the atmospheric accumulation rates of greenhouse Triangle Several inventories of
927 natural and Exposure Assessment global scales have been two classes Fores, *J. Geophys.*
928 *Res.*, 100, 8873–8892, 1995.
- 929 Guenther, A., Karl, T., Harley, P., Wiedinmyer, C., Palmer, P. I., and Geron, C.: Estimates
930 of global terrestrial isoprene emissions using MEGAN (Model of Emissions of Gases and
931 Aerosols from Nature), *Atmos Chem Phys*, 6, 3181–3210, [https://doi.org/10.5194/acpd-6-](https://doi.org/10.5194/acpd-6-107-2006)
932 [107-2006](https://doi.org/10.5194/acpd-6-107-2006), 2006.
- 933 Guenther, A. B. and Hills, A. J.: Eddy covariance measurement of isoprene fluxes, *Journal*
934 *of Geophysical Research Atmospheres*, 103, 13145–13152,
935 <https://doi.org/10.1029/97JD03283>, 1998.
- 936 Guenther, A. B., Zimmerman, P. R., Harley, P. C., Monson, R. K., and Fall, R.: Isoprene
937 and monoterpene emission rate variability - Model evaluation and sensitivity analyses.,
938 *Journal of Geophysical Research-Atmospheres*, 98, 12609–12617, 1993.
- 939 Guenther, A. B., Jiang, X., Heald, C. L., Sakulyanontvittaya, T., Duhl, T., Emmons, L. K.,
940 and Wang, X.: The Model of Emissions of Gases and Aerosols from Nature version 2.1
941 (MEGAN2.1): an extended and updated framework for modeling biogenic emissions,
942 *Geosci Model Dev*, 5, 1503–1560, <https://doi.org/10.5194/gmdd-5-1503-2012>, 2012.
- 943 Harley, P., Vasconcelos, P., Vierling, L., Pinheiro, C. C. D. S., Greenberg, J., Guenther,
944 A., Klinger, L., Almeida, S. S. de, Neill, D., Baker, T., Phillips, O., and Malhi, Y.: Variation
945 in potential for isoprene emissions among Neotropical forest sites, *Glob Chang Biol*, 10,
946 630–650, <https://doi.org/10.1111/j.1529-8817.2003.00760.x>, 2004.
- 947 Harrison, S. P., Dani, K. G. S., Prentice, I. C., Atwell, B. J., Leishman, M. R., Medlyn, B.
948 E., Wright, I. J., Morfopoulos, C., Arneth, A., Barkley, M. P., Loreto, F., Niinemets, Ü.,
949 Possell, M., and Peñuelas, J.: Volatile isoprenoid emissions from plastid to planet, *New*
950 *Phytologist*, 197, 49–57, <https://doi.org/10.1111/nph.12021>, 2013.
- 951 Holst, T., Arneth, A., Hayward, S., Ekberg, A., Mastepanov, M., Jackowicz-Korczynski,
952 M., Friborg, T., Crill, P. M., and Backstrand, K.: BVOC ecosystem flux measurements at
953 a high latitude wetland site, *Atmos Chem Phys*, 10, 1617–1634, 2010.
- 954 Jardine, K., Chambers, J., Alves, E. G., Teixeira, A., Garcia, S., Holm, J., Higuchi, N.,
955 Manzi, A., Abrell, L., Fuentes, J. D., Nielsen, L. K., Torn, M. S., and Vickers, C. E.:
956 Dynamic Balancing of Isoprene Carbon Sources Reflects Photosynthetic and
957 Photorespiratory Responses to Temperature Stress, *Plant Physiol*, 166, 2051–2064,
958 <https://doi.org/10.1104/pp.114.247494>, 2014.
- 959 Jardine, K. J., Jardine, A. B., Holm, J. A., Lombardozzi, D. L., Negron-Juarez, R. I., Martin,
960 S. T., Beller, H. R., Gimenez, B. O., Higuchi, N., and Chambers, J. Q.: Monoterpene
961 ‘thermometer’ of tropical forest-atmosphere response to climate warming, *Plant Cell*
962 *Environ*, 40, 441–452, <https://doi.org/10.1111/pce.12879>, 2017.

- 963 Jensen, N. R., Gruening, C., Goded, I., Müller, M., Hjorth, J., and Wisthaler, A.: Eddy-
964 covariance flux measurements in an Italian deciduous forest using PTR-ToF-MS, PTR-
965 QMS and FIS, *Int J Environ Anal Chem*, 98, 758–788,
966 <https://doi.org/10.1080/03067319.2018.1502758>, 2018.
- 967 Jiménez-Muñoz, J. C., Mattar, C., Barichivich, J., Santamaría-Artigas, A., Takahashi, K.,
968 Malhi, Y., Sobrino, J. A., and Schrier, G. van der: Record-breaking warming and extreme
969 drought in the Amazon rainforest during the course of El Niño 2015–2016,
970 <https://doi.org/10.1038/srep33130>, 2016.
- 971 Karl, T., Potosnak, M., Guenther, A., Clark, D., Walker, J., Herrick, J. D., and Geron, C.:
972 Exchange processes of volatile organic compounds above a tropical rain forest:
973 Implications for modeling tropospheric chemistry above dense vegetation, *J Geophys Res*,
974 109, D18306, <https://doi.org/10.1029/2004JD004738>, 2004.
- 975 Keller, M. and Lerdau, M.: Isoprene emission from tropical forest canopy leaves, *Global*
976 *Biogeochem Cycles*, 13, 19–29, 1999.
- 977 Kesselmeier, J., Ciccioli, P., Kuhn, U., Stefani, P., Biesenthal, T., Rottenberger, S., Wolf,
978 A., Vitullo, M., Valentini, R., Nobre, A., Kabat, P., and Andreae, M. O.: Volatile organic
979 compound emissions in relation to plant carbon fixation and the terrestrial carbon budget,
980 *Global Biogeochem Cycles*, 16, 73-1-73-9, <https://doi.org/10.1029/2001GB001813>, 2002.
- 981 Klinger, L. F., Li, Q. J., Guenther, A. B., Greenberg, J. P., Baker, B., and Bai, J. H.:
982 Assessment of volatile organic compound emissions from ecosystems of China, *J Geophys*
983 *Res*, 107, 4603, <https://doi.org/10.1029/2001JD001076>, 2002.
- 984 Kljun, N., Calanca, P., Rotach, M. W., and Schmid, H. P.: A simple two-dimensional
985 parameterisation for Flux Footprint Prediction (FFP), *Geosci Model Dev*, 8, 3695–3713,
986 <https://doi.org/10.5194/gmd-8-3695-2015>, 2015.
- 987 Kuhn, U., Rottenberger, S., Biesenthal, T., Wolf, a., Schebeske, G., Ciccioli, P.,
988 Brancaleoni, E., Frattoni, M., Tavares, T. M., and Kesselmeier, J.: Seasonal differences in
989 isoprene and light-dependent monoterpene emission by Amazonian tree species, *Glob*
990 *Chang Biol*, 10, 663–682, <https://doi.org/10.1111/j.1529-8817.2003.00771.x>, 2004a.
- 991 Kuhn, U., Rottenberger, S., Biesenthal, T., Wolf, A., Schebeske, G., Ciccioli, P., and
992 Kesselmeier, J.: Strong correlation between isoprene emission and gross photosynthetic
993 capacity during leaf phenology of the tropical tree species *Hymenaea courbaril* with
994 fundamental changes in volatile organic compounds emission composition during early
995 leaf development, *Plant Cell Environ*, 27, 1469–1485, <https://doi.org/10.1111/j.1365-3040.2004.01252.x>, 2004b.
- 997 Langford, B., House, E., Valach, A., Hewitt, C. N., Artaxo, P., Barkley, M. P., Brito, J.,
998 Carnell, E., Davison, B., MacKenzie, A. R., Marais, E. A., Newland, M. J., Rickard, A. R.,
999 Shaw, M. D., Yáñez-Serrano, A. M., and Nemitz, E.: Seasonality of isoprene emissions
1000 and oxidation products above the remote Amazon, *Environmental Science: Atmospheres*,
1001 2, 230–240, <https://doi.org/10.1039/D1EA00057H>, 2022.
- 1002 Lerdau, M. and Keller, M.: Controls on isoprene emission from trees in a subtropical dry
1003 forest, *Plant Cell Environ*, 20, 569–578, <https://doi.org/10.1111/j.1365-3040.1997.00075.x>, 1997.
- 1005 Lopes, A. P., Nelson, B. W., Wu, J., Graça, P. M. L. de A., Tavares, J. V., Prohaska, N.,
1006 Martins, G. A., and Saleska, S. R.: Leaf flush drives dry season green-up of the Central
1007 Amazon, *Remote Sens Environ*, 182, 90–98, <https://doi.org/10.1016/j.rse.2016.05.009>,
1008 2016.

- 1009 Malhi, Y., Roberts, J. T., Betts, R. A., Killeen, T. J., Li, W. H., and Nobre, C. A.: Climate
1010 change, deforestation, and the fate of the Amazon, *Science* (1979), 319, 169–172,
1011 <https://doi.org/10.1126/science.1146961>, 2008.
- 1012 Mauder, T. and Foken, T.: *Documentation and Instruction Manual of the Eddy Covariance*
1013 *Software Package TK2*, Bayreuth: Universität Bayreuth, 2004.
- 1014 Monson, R. K., Jones, R. T., Rosenstiel, T. N., and Schnitzler, J. P.: Why only some plants
1015 emit isoprene, *Plant Cell Environ*, 36, 503–516, <https://doi.org/10.1111/pce.12015>, 2013.
- 1016 Niinemets, Ü.: Leaf age dependent changes in within-canopy variation in leaf functional
1017 traits: a meta-analysis, *J Plant Res*, 129, 313–338, [https://doi.org/10.1007/s10265-016-](https://doi.org/10.1007/s10265-016-0815-2)
1018 [0815-2](https://doi.org/10.1007/s10265-016-0815-2), 2016.
- 1019 Niinemets, U., Monson, R. K., Arneth, A., Ciccioli, P., Kesselmeier, J., Kuhn, U., Noe, S.
1020 M., Penuelas, J., and Staudt, M.: The leaf-level emission factor of volatile isoprenoids:
1021 caveats, model algorithms, response shapes and scaling, *Biogeosciences*, 7, 1809–1832,
1022 <https://doi.org/10.5194/bg-7-1809-2010>, 2010.
- 1023 Nobre, C. A., Sampaio, G., Borma, L. S., Castilla-Rubio, J. C., Silva, J. S., and Cardoso,
1024 M.: Land-use and climate change risks in the Amazon and the need of a novel sustainable
1025 development paradigm, *Proceedings of the National Academy of Sciences*, 113,
1026 <https://doi.org/10.1073/pnas.1605516113>, 2016.
- 1027 Nölscher, A. C., Yáñez-Serrano, A. M., Wolff, S., de Araujo, A. C., Lavrič, J. v.,
1028 Kesselmeier, J., and Williams, J.: Unexpected seasonality in quantity and composition of
1029 Amazon rainforest air reactivity, *Nat Commun*, 7, 10383,
1030 <https://doi.org/10.1038/ncomms10383>, 2016.
- 1031 Padhy, P. K. and Varshney, C. K.: Isoprene emission from tropical tree species,
1032 *Environmental Pollution*, 135, 101–109, <https://doi.org/10.1016/j.envpol.2004.10.003>,
1033 2005.
- 1034 Pegoraro, E., Rey, A., Abrell, L., Haren, J., and Lin, G.: Drought effect on isoprene
1035 production and consumption in Biosphere 2 tropical rainforest, *Glob Chang Biol*, 12, 456–
1036 469, <https://doi.org/10.1111/j.1365-2486.2006.01112.x>, 2006.
- 1037 Pfannerstill, E. Y., Nölscher, A. C., Yáñez-Serrano, A. M., Bourtsoukidis, E., Keßel, S.,
1038 Janssen, R. H. H., Tsokankunku, A., Wolff, S., Sörgel, M., Sá, M. O., Araújo, A., Walter,
1039 D., Lavrič, J., Dias-Júnior, C. Q., Kesselmeier, J., and Williams, J.: Total OH Reactivity
1040 Changes Over the Amazon Rainforest During an El Niño Event, *Frontiers in Forests and*
1041 *Global Change*, 1, <https://doi.org/10.3389/ffgc.2018.00012>, 2018a.
- 1042 Pfannerstill, E. Y., Nölscher, A. C., Yáñez-Serrano, A. M., Bourtsoukidis, E., Keßel, S.,
1043 Janssen, R. H. H., Tsokankunku, A., Wolff, S., Sörgel, M., Sá, M. O., Araújo, A., Walter,
1044 D., Lavrič, J., Dias-Júnior, C. Q., Kesselmeier, J., and Williams, J.: Total OH Reactivity
1045 Changes Over the Amazon Rainforest During an El Niño Event, *Frontiers in Forests and*
1046 *Global Change*, 1, 1–17, <https://doi.org/10.3389/ffgc.2018.00012>, 2018b.
- 1047 Pfannerstill, E. Y., Reijrink, N. G., Edtbauer, A., Ringsdorf, A., Zannoni, N., Araújo, A.,
1048 Ditas, F., Holanda, B. A., Sá, M. O., Tsokankunku, A., Walter, D., Wolff, S., Lavri, J. v.,
1049 Pöhlker, C., Sörgel, M., and Williams, J.: Total OH reactivity over the Amazon rainforest:
1050 Variability with temperature, wind, rain, altitude, time of day, season, and an overall budget
1051 closure, *Atmos Chem Phys*, 21, 6231–6256, <https://doi.org/10.5194/acp-21-6231-2021>,
1052 2021.
- 1053 Pöhlker, C., Walter, D., Paulsen, H., Könnemann, T., Rodríguez-caballero, E., Moran-
1054 zuloaga, D., Brito, J., Carbone, S., Degrendele, C., Després, V. R., Ditas, F., Pöhlker, M.

1055 L., Praß, M., Löbs, N., Saturno, J., Sörgel, M., Wang, Q., Weber, B., Wolff, S., Artaxo, P.,
1056 Pöschl, U., and Andreae, M. O.: Land cover and its transformation in the backward
1057 trajectory footprint region of the Amazon Tall Tower Observatory, 8425–8470, 2019.
1058 Poschl, U., Martin, S. T., Sinha, B., Chen, Q., Gunthe, S. S., Huffman, J. A., Borrmann, S.,
1059 Farmer, D. K., Garland, R. M., Helas, G., Jimenez, J. L., King, S. M., Manzi, A.,
1060 Mikhailov, E., Pauliquevis, T., Petters, M. D., Prenni, A. J., Roldin, P., Rose, D., Schneider,
1061 J., Su, H., Zorn, S. R., Artaxo, P., and Andreae, M. O.: Rainforest Aerosols as Biogenic
1062 Nuclei of Clouds and Precipitation in the Amazon, *Science* (1979), 329, 1513–1516,
1063 <https://doi.org/10.1126/science.1191056>, 2010.
1064 Rodrigues, T. B., Baker, C. R., Walker, A. P., McDowell, N., Rogers, A., Higuchi, N.,
1065 Chambers, J. Q., and Jardine, K. J.: Stimulation of isoprene emissions and electron
1066 transport rates as key mechanisms of thermal tolerance in the tropical species *Vismia*
1067 *guianensis*, *Glob Chang Biol*, 26, 5928–5941, <https://doi.org/10.1111/gcb.15213>, 2020.
1068 Sindelarova, K., Granier, C., Bouarar, I., Guenther, a., Tilmes, S., Stavrakou, T., Müller,
1069 J.-F., Kuhn, U., Stefani, P., and Knorr, W.: Global data set of biogenic VOC emissions
1070 calculated by the MEGAN model over the last 30 years, *Atmos Chem Phys*, 14, 9317–
1071 9341, <https://doi.org/10.5194/acp-14-9317-2014>, 2014.
1072 Spirig, C., Neftel, A., Ammann, C., Dommen, J., Grabmer, W., Thielmann, A., Schaub,
1073 A., Beauchamp, J., Wisthaler, A., and Hansel, A.: Eddy covariance flux measurements of
1074 biogenic VOCs during ECHO 2003 using proton transfer reaction mass spectrometry,
1075 *Atmos Chem Phys*, 5, 465–481, <https://doi.org/10.5194/acp-5-465-2005>, 2005.
1076 Stark, S. C., Leitold, V., Wu, J. L., Hunter, M. O., de Castilho, C. V., Costa, F. R. C.,
1077 McMahon, S. M., Parker, G. G., Shimabukuro, M. T., Lefsky, M. a, Keller, M., Alves, L.
1078 F., Schiatti, J., Shimabukuro, Y. E., Brandão, D. O., Woodcock, T. K., Higuchi, N., de
1079 Camargo, P. B., de Oliveira, R. C., Saleska, S. R., and Chave, J.: Amazon forest carbon
1080 dynamics predicted by profiles of canopy leaf area and light environment., *Ecol Lett*, 15,
1081 1406–14, <https://doi.org/10.1111/j.1461-0248.2012.01864.x>, 2012.
1082 ter Steege, H., Pitman, N. C. A., Sabatier, D., Baraloto, C., Salomao, R. P., Guevara, J. E.,
1083 Phillips, O. L., Castilho, C. v, Magnusson, W. E., Molino, J.-F., Monteagudo, A., Nunez
1084 Vargas, P., Montero, J. C., Feldpausch, T. R., Coronado, E. N. H., Killeen, T. J.,
1085 Mostacedo, B., Vasquez, R., Assis, R. L., Terborgh, J., Wittmann, F., Andrade, A.,
1086 Laurance, W. F., Laurance, S. G. W., Marimon, B. S., Marimon, B.-H., Guimaraes Vieira,
1087 I. C., Amaral, I. L., Brienen, R., Castellanos, H., Cardenas Lopez, D., Duivenvoorden, J.
1088 F., Mogollon, H. F., Matos, F. D. de A., Davila, N., Garcia-Villacorta, R., Stevenson Diaz,
1089 P. R., Costa, F., Emilio, T., Levis, C., Schiatti, J., Souza, P., Alonso, A., Dallmeier, F.,
1090 Montoya, A. J. D., Fernandez Piedade, M. T., Araujo-Murakami, A., Arroyo, L., Gribel,
1091 R., Fine, P. V. A., Peres, C. A., Toledo, M., Aymard C., G. A., Baker, T. R., Ceron, C.,
1092 Engel, J., Henkel, T. W., Maas, P., Petronelli, P., Stropp, J., Zartman, C. E., Daly, D., Neill,
1093 D., Silveira, M., Paredes, M. R., Chave, J., Lima Filho, D. de A., Jorgensen, P. M., Fuentes,
1094 A., Schongart, J., Cornejo Valverde, F., di Fiore, A., Jimenez, E. M., Penuela Mora, M. C.,
1095 Phillips, J. F., Rivas, G., van Andel, T. R., von Hildebrand, P., Hoffman, B., Zent, E. L.,
1096 Malhi, Y., Prieto, A., Rudas, A., Ruschell, A. R., Silva, N., Vos, V., Zent, S., Oliveira, A.
1097 A., Schutz, A. C., Gonzales, T., Trindade Nascimento, M., Ramirez-Angulo, H., Sierra, R.,
1098 Tirado, M., Umana Medina, M. N., van der Heijden, G., Vela, C. I. A., Vilanova Torre, E.,
1099 Vriesendorp, C., et al.: Hyperdominance in the Amazonian Tree Flora, *Science* (1979),
1100 342, 1243092–1243092, <https://doi.org/10.1126/science.1243092>, 2013.

- 1101 Tambunan, P., Baba, S., Kuniyoshi, A., Iwasaki, H., Nakamura, T., Yamasaki, H., and
1102 Oku, H.: Isoprene emission from tropical trees in Okinawa Island, Japan, *Chemosphere*,
1103 65, 2138–2144, <https://doi.org/10.1016/j.chemosphere.2006.06.013>, 2006.
- 1104 Taylor, T. C., McMahon, S. M., Smith, M. N., Boyle, B., Violle, C., van Haren, J., Simova,
1105 I., Meir, P., Ferreira, L. v., de Camargo, P. B., da Costa, A. C. L., Enquist, B. J., and
1106 Saleska, S. R.: Isoprene emission structures tropical tree biogeography and community
1107 assembly responses to climate, *New Phytologist*, 220, 435–446,
1108 <https://doi.org/10.1111/nph.15304>, 2018.
- 1109 Taylor, T. C., Smith, M. N., Slot, M., and Feeley, K. J.: The capacity to emit isoprene
1110 differentiates the photosynthetic temperature responses of tropical plant species, *Plant Cell
1111 Environ*, 42, 2448–2457, <https://doi.org/10.1111/pce.13564>, 2019.
- 1112 Taylor, T. C., Wisniewski, W. T., Alves, E. G., Oliveira Junior, R. C., and Saleska, S. R.:
1113 A New Field Instrument for Leaf Volatiles Reveals an Unexpected Vertical Profile of
1114 Isoprenoid Emission Capacities in a Tropical Forest, *Frontiers in Forests and Global
1115 Change*, 4, 1–22, <https://doi.org/10.3389/ffgc.2021.668228>, 2021.
- 1116 Varshney, C. K. and Singh, A. P.: Isoprene emission from Indian trees, *J Geophys Res*,
1117 108, 4803, <https://doi.org/10.1029/2003JD003866>, 2003.
- 1118 Vickers, D. and Mahrt, L.: Quality control and flux sampling problems for tower and
1119 aircraft data, *J Atmos Ocean Technol*, 14, 512–526, [https://doi.org/10.1175/1520-0426\(1997\)014<0512:QCAFSP>2.0.CO;2](https://doi.org/10.1175/1520-0426(1997)014<0512:QCAFSP>2.0.CO;2), 1997.
- 1121 Wei, D., Fuentes, J. D., Gerken, T., Chamecki, M., Trowbridge, A. M., Stoy, P. C., Katul,
1122 G. G., Fisch, G., Acevedo, O., Manzi, A., von Randow, C., and dos Santos, R. M. N.:
1123 Environmental and biological controls on seasonal patterns of isoprene above a rain forest
1124 in central Amazonia, *Agric For Meteorol*, 256–257, 391–406,
1125 <https://doi.org/10.1016/j.agrformet.2018.03.024>, 2018.
- 1126 Wells, K. C., Millet, D. B., Payne, V. H., Vigouroux, C., Aquino, C. A. B., Mazière, M.,
1127 Gouw, J. A., Graus, M., Kurosu, T., Warneke, C., and Wisthaler, A.: Next-Generation
1128 Isoprene Measurements From Space: Detecting Daily Variability at High Resolution,
1129 *Journal of Geophysical Research: Atmospheres*, 127,
1130 <https://doi.org/10.1029/2021JD036181>, 2022.
- 1131 Werner, C., Meredith, L. K., Ladd, S. N., Ingrisich, J., Kübert, A., van Haren, J., Bahn, M.,
1132 Bailey, K., Bamberger, I., Beyer, M., Blomdahl, D., Byron, J., Daber, E., Deleeuw, J.,
1133 Dippold, M. A., Fudyma, J., Gil-Loaiza, J., Honeker, L. K., Hu, J., Huang, J., Klüpfel, T.,
1134 Krechmer, J., Kreuzwieser, J., Kühnhammer, K., Lehmann, M. M., Meeran, K., Misztal,
1135 P. K., Ng, W.-R., Pfannerstill, E., Pugliese, G., Purser, G., Roscioli, J., Shi, L., Tfaily, M.,
1136 and Williams, J.: Ecosystem fluxes during drought and recovery in an experimental forest,
1137 *Science* (1979), 374, 1514–1518, <https://doi.org/10.1126/science.abj6789>, 2021.
- 1138 Wu, J., Albert, L. P., Lopes, A. P., Restrepo-Coupe, N., Hayek, M., Wiedemann, K. T.,
1139 Guan, K., Stark, S. C., Christoffersen, B., Prohaska, N., Tavares, J. v., Marostica, S.,
1140 Kobayashi, H., Ferreira, M. L., Campos, K. S., Silva, R. da, Brando, P. M., Dye, D. G.,
1141 Huxman, T. E., Huete, A. R., Nelson, B. W., and Saleska, S. R.: Leaf development and
1142 demography explain photosynthetic seasonality in Amazon evergreen forests, *Science*
1143 (1979), 351, 972–976, <https://doi.org/10.1126/science.aad5068>, 2016a.
- 1144 Wu, J., Albert, L. P., Lopes, A. P., Restrepo-Coupe, N., Hayek, M., Wiedemann, K. T.,
1145 Guan, K., Stark, S. C., Christoffersen, B., Prohaska, N., Tavares, J. v., Marostica, S.,
1146 Kobayashi, H., Ferreira, M. L., Campos, K. S., da Silva, R., Brando, P. M., Dye, D. G.,

1147 Huxman, T. E., Huete, A. R., Nelson, B. W., and Saleska, S. R.: Leaf development and
1148 demography explain photosynthetic seasonality in Amazon evergreen forests, *Science*
1149 (1979), 351, 972–976, <https://doi.org/10.1126/science.aad5068>, 2016b.
1150 Yáñez-Serrano, A. M., Nölscher, A. C., Williams, J., Wolff, S., Alves, E., Martins, G. A.,
1151 Bourtsoukidis, E., Brito, J., Jardine, K., Artaxo, P., and Kesselmeier, J.: Diel and seasonal
1152 changes of biogenic volatile organic compounds within and above an Amazonian
1153 rainforest, *Atmos Chem Phys*, 15, 3359–3378, <https://doi.org/10.5194/acp-15-3359-2015>,
1154 2015.
1155 Yáñez-Serrano, A. M., Nölscher, A. C., Bourtsoukidis, E., Gomes Alves, E., Ganzeveld,
1156 L., Bonn, B., Wolff, S., Sa, M., Yamasoe, M., Williams, J., Andreae, M. O., and
1157 Kesselmeier, J.: Monoterpene chemical speciation in the Amazon tropical rainforest:
1158 variation with season, height, and time of day at the Amazon Tall Tower Observatory
1159 (ATTO), *Atmos Chem Phys*, 18, 3403–3418, <https://doi.org/10.5194/acp-2017-817>, 2018.
1160 Yáñez-Serrano, A. M., Bourtsoukidis, E., Alves, E. G., Bauwens, M., Stavrakou, T., Llusà,
1161 J., Filella, I., Guenther, A., Williams, J., Artaxo, P., Sindelarova, K., Doubalova, J.,
1162 Kesselmeier, J., and Peñuelas, J.: Amazonian biogenic volatile organic compounds under
1163 global change, *Glob Chang Biol*, 26, 4722–4751, <https://doi.org/10.1111/gcb.15185>, 2020.
1164 Zannoni, N., Leppla, D., Lembo Silveira de Assis, P. I., Hoffmann, T., Sá, M., Araújo, A.,
1165 and Williams, J.: Surprising chiral composition changes over the Amazon rainforest with
1166 height, time and season, *Commun Earth Environ*, 1, 1–11, <https://doi.org/10.1038/s43247-020-0007-9>, 2020.
1167
1168
1169
1170
1171
1172
1173
1174
1175
1176
1177
1178
1179
1180
1181
1182
1183
1184
1185
1186
1187
1188
1189
1190
1191
1192

1193 **Tables**

1194

1195 **Table 1.** Isoprene mixing ratios (ppbv) at 38 m for all field campaigns. Mixing ratios are
1196 mean values of isoprene measured at 12:00-15:00, local time (UTC-4h). Values within
1197 brackets are one standard deviation of the mean and the number of sampling days for each
1198 campaign.

Year	Month	Season	Isoprene (ppbv) at 38 m
2012	November	dry-to-wet transition season	9.30 (4.90) (n=4 days)
2013	February	wet season	1.10 (0.66) (n=6 days)
2013	March	wet season	1.84 (1.44) (n=3 days)
2013	June	wet-to-dry transition season	1.83 (0.82) (n=5 days)
2013	September	dry season	5.02 (1.99) (n=8 days)
2014	February	wet season	5.92 (4.89) (n=3 days)
2014	March	wet season	2.92 (2.50) (n=11 days)
2014	August	dry season	7.76 (2.49) (n=15 days)
2015	October	dry season – <i>El-Niño</i> year	8.94 (1.41) (n=13 days)

1199
1200
1201
1202
1203
1204
1205
1206
1207
1208
1209
1210
1211
1212
1213
1214
1215
1216
1217
1218
1219
1220
1221
1222
1223
1224
1225
1226

1227 **Table 2.** Model parameters for all simulations for the years 2014 and 2015.

	1 st model simulation (S1)	2 nd model simulation (S2)	3 rd model simulation (S3)	4 th model simulation (S4)
PPFD and air temperature	30 min averages – tower measurements	30 min averages – tower measurements	30 min averages – tower measurements	30 min averages – tower measurements
β^1	0.13	0.13	0.13	0.13
LDF ²	1	1	1	1
C_{tl}^3	95	95	95	95
C_{eo}^4	2	2	2	2
Isoprene emission factor (E_s)	7 mg m ⁻² h ⁻¹	7 mg m ⁻² h ⁻¹	3.21 mg m ⁻² h ⁻¹	3.21 mg m ⁻² h ⁻¹
LAI	5.32	5.32	5.32	5.32
Leaf age algorithm – LAI	default	Modified with leaf age classes derived from the phenocam: <i>young leaves (0–1 month), growing (1–2 months), mature leaves (3–6 months), old leaves (>6 months).</i>	Modified with leaf age classes derived from the phenocam: <i>young leaves (0–1 month), growing (1–2 months), mature leaves (3–6 months), old leaves (>6 months).</i>	Modified with leaf age classes derived from the phenocam: <i>young leaves (0–1 month), growing (1–2 months), mature leaves (3–6 months), old leaves (>6 months).</i>
Leaf age emission activity factor	default $A_{new}=0.05$ $A_{gro}=0.6$ $A_{mat}=1$ $A_{old}=0.9$	default $A_{new}=0.05$ $A_{gro}=0.6$ $A_{mat}=1$ $A_{old}=0.9$	default $A_{new}=0.05$ $A_{gro}=0.6$ $A_{mat}=1$ $A_{old}=0.9$	modified according to leaf-level measurements: $A_{new}=0.01$ $A_{gro}=1$ $A_{mat}=1$ $A_{old}=0.64$

1228 *Note:* Empirical coefficients are from Guenther et al. (2012)

1229 1. Temperature empirical coefficient

1230 2. Light-dependent fraction

1231 3. Temperature empirical coefficient

1232 4. Emission-class dependent empirical coefficient

1233

1234

1235

1236

1237

1238

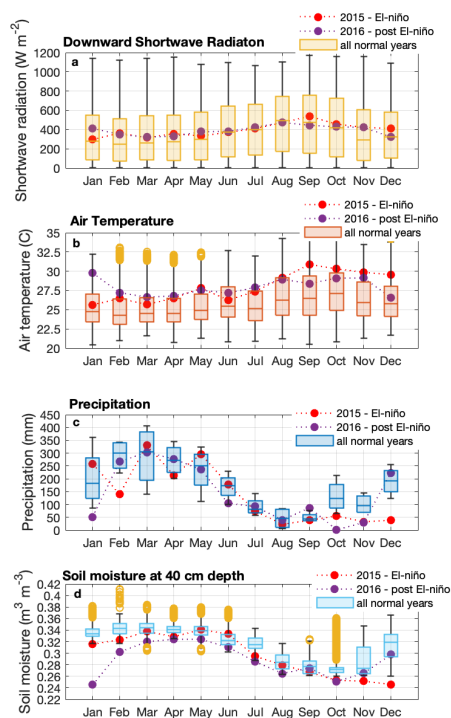
1239

1240

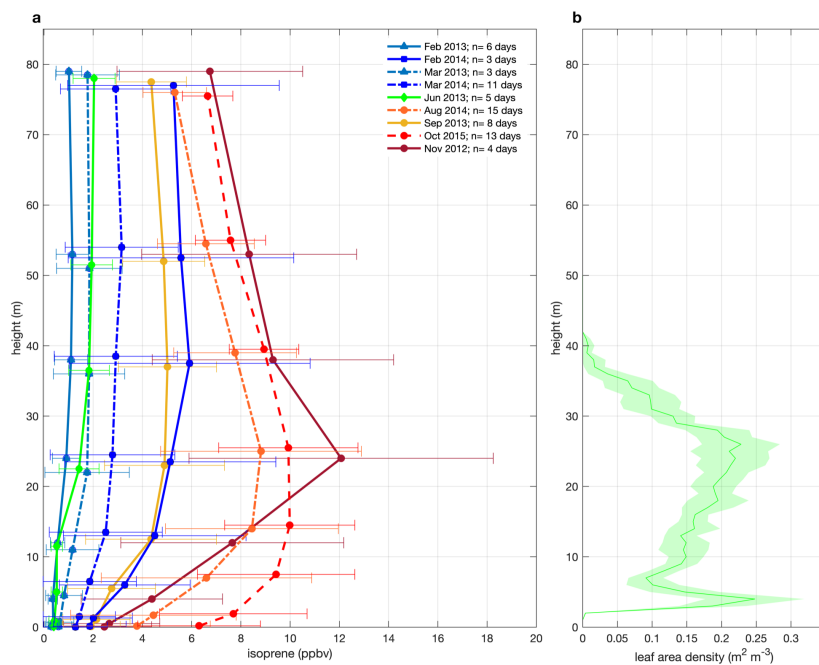
1241

1242

1243
1244 **Figures**
1245

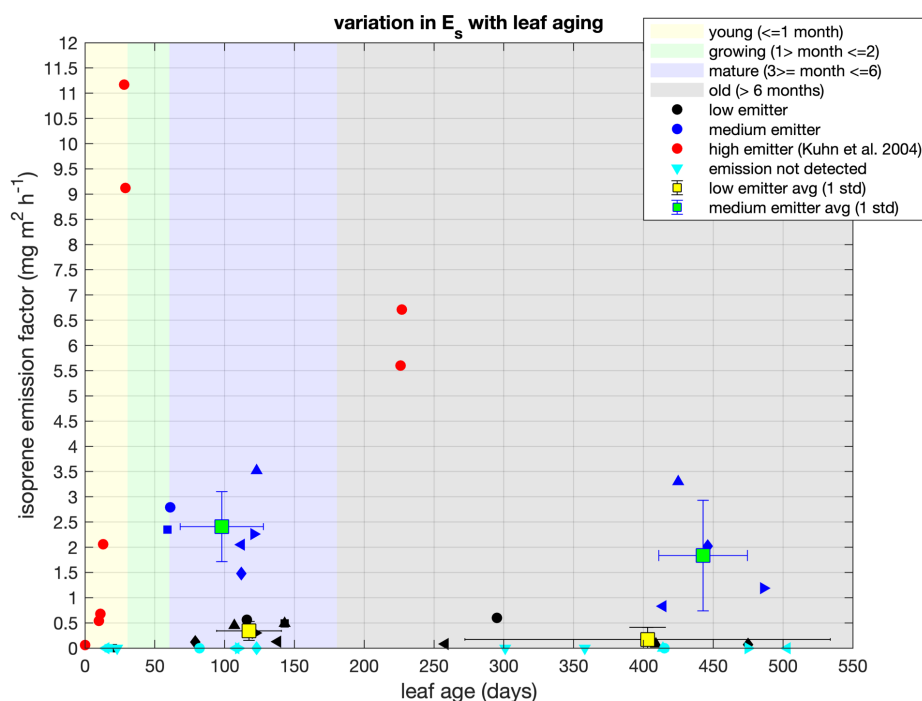


1246
1247 **Figure 1.** Seasonal variation of solar radiation (a), air temperature (b), precipitation (c), and soil
1248 moisture (d) during normal years (2013, 2014, 2017, 2018, and 2019), an El-niño (2015), and post-
1249 El-niño year (2016) - measured at the ATTO site. Boxplots present the median, the lower, and the
1250 upper quartiles, where the upper quartile corresponds to the 0.75 quantile and the lower quartile
1251 corresponds to the 0.25 quantile; whiskers connect the upper quartile and lower quartile to the
1252 maximum and minimum nonoutliers, respectively; and outliers are values that are more than
1253 $1.5 \cdot \text{IQR}$ (interquartile range) away from the top or bottom of the box.
1254
1255
1256
1257
1258
1259
1260
1261
1262
1263
1264



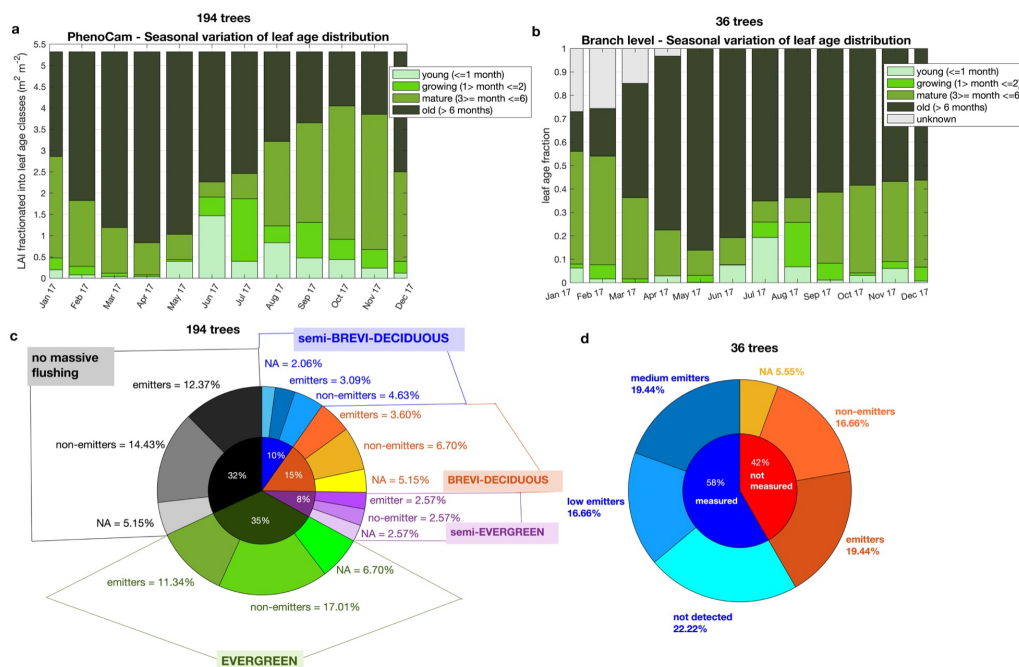
1265
1266 **Figure 2.** Mean isoprene mixing ratios for all field campaigns from Nov 2012 to Oct 2015, with
1267 one standard deviation - 12:00-15:00 local time, UTC-4h - a daytime period that isoprene emission
1268 is the highest; and mean canopy leaf area density profile with a confidence interval of 95% (b).
1269 The measurements of all intensive campaigns were collected at the same heights (0.05, 0.5,
1270 4, 12, 24, 38, 53, and 79 m), but note that in the plot (a) the heights were shifted by 50 cm
1271 only for the better visualization of the error bars.

1272
1273
1274
1275
1276
1277
1278
1279
1280
1281
1282
1283
1284
1285
1286
1287
1288



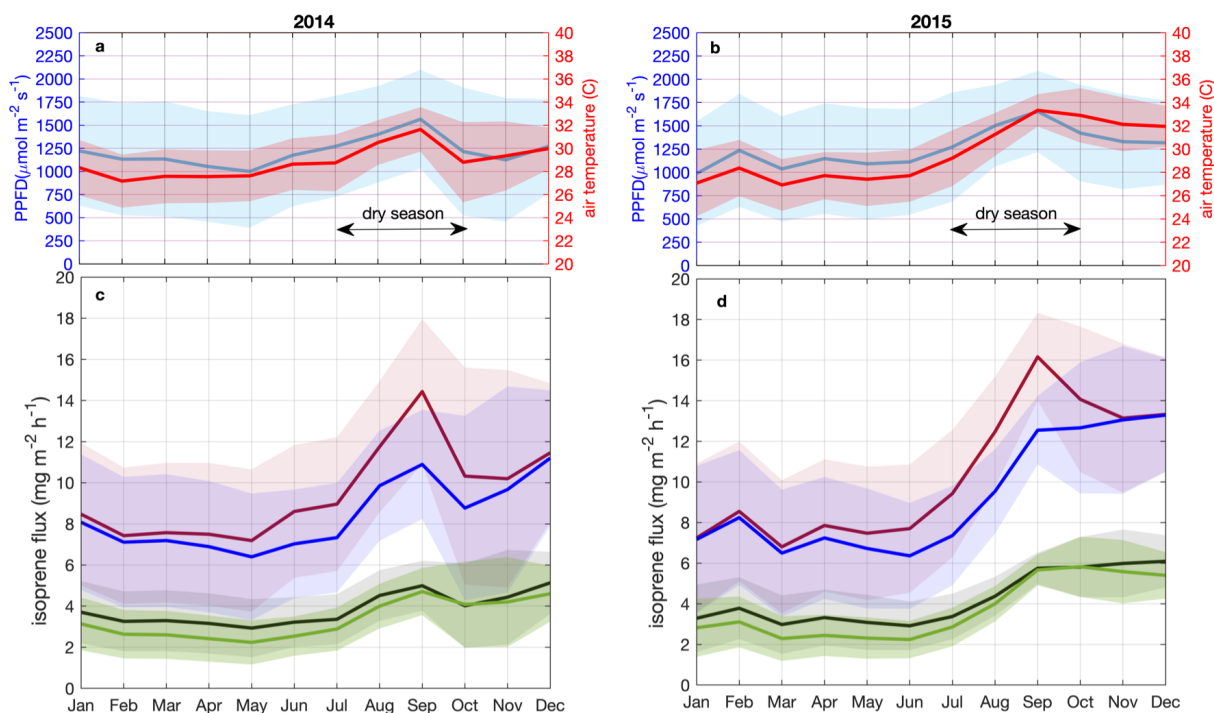
1289
1290 **Figure 3.** Isoprene emission factor (E_s) across leaf age classes and characterized into qualitative
1291 emission categories – low, medium, and high. Measured tree species were categorized into
1292 medium (blue) and low (black) emitters according to their E_s values, and different symbols
1293 represent different tree species. The high emitter category (red) represents a tropical species
1294 measured in Kuhn et al. (2004b). Values represent observations of individual trees, and mean
1295 and one standard deviation for the categories medium and low emitters at mature and old leaf age
1296 classes. Shade areas represent the intervals of days for each leaf age class.

1297
1298
1299
1300
1301
1302
1303
1304
1305
1306
1307
1308
1309
1310
1311
1312
1313
1314



1314
 1316
 1317
 1318
 1319
 1320
 1321
 1322
 1323
 1324
 1325
 1326
 1327
 1328
 1329
 1330
 1331
 1332
 1333
 1334
 1335
 1336
 1337
 1338
 1339
 1340
 1341
 1342

Figure 4. Leaf phenology and demography and isoprene emission trait. Panel (a) shows the leaf age distribution fractionated into LAI that was observed with the phenocam, in 2017; and panel (b) shows the leaf age distribution observed at branch level for 36 trees, in 2017 - note that unknown age refers to leaves that were attached to the branch at the beginning of monitoring and therefore could not be assigned to an age class. Panel (c) shows the percentual distribution of the phenotypes assigned to the 194 trees observed with the phenocam – no massive flushing, evergreen, semi-evergreen, deciduous, and semi-brevideciduous –, and the emission trait assigned to each tree species within these phenotypes – emitters, non-emitters, and NA (NA=no data available). Panel (d) presents the percentual distribution of the isoprene trait estimated to the non-measured trees (red); and the isoprene emission trait within measured tree species (blue), with measured tree species being categorized in classes of medium emission, low emission and not detected emission.

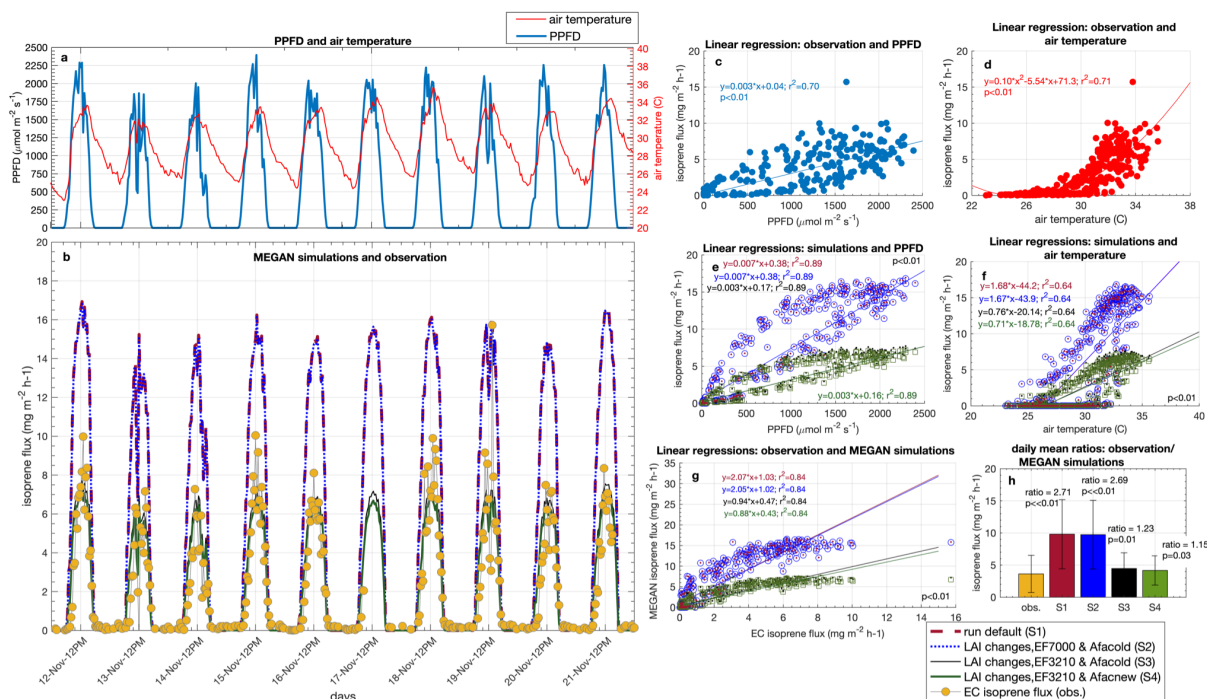


- S1: MEGAN simulation default (no change in the LAI code, $EF=7 \text{ mg m}^{-2} \text{ h}^{-1}$ and leaf age activity factor unmodified)
- S2: MEGAN simulation with change for LAI - leaf age classes, $EF=7 \text{ mg m}^{-2} \text{ h}^{-1}$ and leaf age activity factor unmodified
- S3: MEGAN simulation with change for LAI - leaf age classes, $EF=3.21 \text{ mg m}^{-2} \text{ h}^{-1}$ and leaf age activity factor unmodified
- S4: MEGAN simulation with change for LAI - leaf age classes, $EF=3.21 \text{ mg m}^{-2} \text{ h}^{-1}$ and leaf age activity factor modified

1344 **Figure 5.** Simulated isoprene emission flux for 2014 and 2015. Monthly average of PPFD and air
 1345 temperature (a, b) measured at the INSTANT tower. Simulations for 2014 (c) and 2015 (d) are:
 1346 MEGAN simulation default, no change in the LAI code, emission factor equals to $7 \text{ mg m}^{-2} \text{ h}^{-1}$ and
 1347 leaf age activity factor unmodified - S1; MEGAN simulation with change for LAI - leaf age classes,
 1348 emission factor equals to $7 \text{ mg m}^{-2} \text{ h}^{-1}$ and leaf age activity factor unmodified - S2; MEGAN
 1349 simulation with change for LAI - leaf age classes, emission factor equals to $3.21 \text{ mg m}^{-2} \text{ h}^{-1}$ and
 1350 leaf age activity factor unmodified - S3; MEGAN simulation with change for LAI - leaf age classes,
 1351 emission factor equals to $3.21 \text{ mg m}^{-2} \text{ h}^{-1}$ and leaf age activity factor modified - S4. Solid lines are
 1352 means, and shaded areas represent one standard deviation of the mean.

1353
 1354
 1355
 1356
 1357
 1358
 1359
 1360
 1361
 1362
 1363
 1364

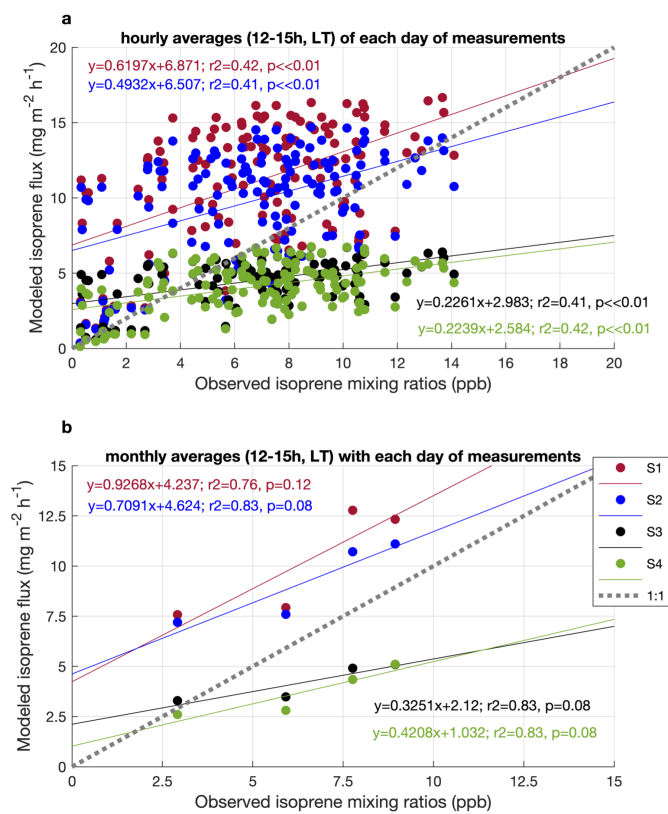
1365



1367 **Figure 6.** Observation of isoprene flux (eddy covariance) and MEGAN simulation for 11 days
 1368 in November 2015. Half-hourly averages of PPFD and air temperature (a); EC isoprene flux and
 1369 MEGAN simulations (b); linear regression between EC isoprene flux and PPFD (c); linear
 1370 regression between EC isoprene flux and air temperature (d); linear regression between simulations
 1371 and PPFD (e); linear regression between simulations and air temperature (f); linear regression
 1372 between EC isoprene flux and simulations (g); daily mean ratios between observation and
 1373 simulations (h).

1374
 1375
 1376
 1377
 1378
 1379
 1380
 1381
 1382
 1383
 1384
 1385
 1386
 1387
 1388
 1389
 1390

1391



1392

1393 **Figure 7.** Correlation between isoprene mixing ratios observed at 38m during Feb and Mar

1394 2014, Aug 2014, and Oct 2015, and the four simulations done for the respective periods.

1395 Hourly averages (12-15h, local time (LT)) of each day of measurements (a); and monthly

1396 averages (12-15h, local time (LT)) with each day of measurements (b).

1397

1398

1399

1400

1401

1402

1403

1404

1405

1406

1407

1408

1409